Structural study of the Eu^{3+} environments in fluorozirconate glasses: Role of the temperature-induced and the pressure-induced phase transition processes in the development of a rare earth's local structure model

Juan E. Muñoz-Santiuste,[1] Ulises R. Rodríguez-Mendoza,[2] Javier González-Platas,[3] and Víctor Lavín[2,a)]

[1]*Departamento de Física Aplicada and MALTA Consolider Team, Escuela Politécnica Superior, Universidad Carlos III de Madrid, Avenida del Mediterráneo 20, E-28913 Leganés, Madrid, Spain*
[2]*Departamento de Física Fundamental y Experimental, Electrónica y Sistemas and MALTA Consolider Team, Universidad de La Laguna, E-38200 San Cristóbal de La Laguna, Santa Cruz de Tenerife, Spain*
[3]*Departamento de Física Fundamental II and MALTA Consolider Team, Universidad de La Laguna, E-38200 San Cristóbal de La Laguna, Santa Cruz de Tenerife, Spain*

(Received 17 December 2008; accepted 22 February 2009; published online 15 April 2009)

The correlation between the optical properties of the Eu^{3+} ions and their local structures in fluorozirconate glasses and glass-ceramics have been analyzed by means of steady-state and time-resolved site-selective laser spectroscopies. Changes in the crystal-field interaction, ranging from weak to medium strength values, are observed monitoring the luminescence and the lifetime of the Eu^{3+} ions in different local environments in the glass. As key roles in this study, the Eu^{3+} luminescence in the thermally-induced crystallization of the glass and the pressure-induced amorphization of the crystalline phase of the glass-ceramic experimentally states the existence of a parent local structure for the Eu^{3+} ions in the glass, identified as the $EuZrF_7$ crystalline phase. Starting from the *ab initio* single overlap model, crystal-field calculations have been performed in the glass and the glass-ceramic. From the site-selective measurements, the crystal-field parameters sets are obtained, giving a suitable simulation of the ^7F_J $(J=0-6)$ Stark energy level diagram for the Eu^{3+} ions in the different environments present in the fluorozirconate glass. A simple geometrical model based on a continuous distortion of the parent structure is proposed for the distribution of local environments of the Eu^{3+} ions in the fluorozirconate glass. © *2009 American Institute of Physics*. [DOI: 10.1063/1.3100770]

I. INTRODUCTION

The optical properties and the structure of the different families of fluoride glasses, especially heavy metal fluoride glasses, have been extensively investigated since their discovery in 1970s. Their relatively low-energy phonons (≤ 500 cm^{-1}), compared to oxide glasses, and high optical transparency from mid-UV to mid-IR make them good materials in the fabrication of optical fibers, optical waveguides and IR optoelectronic devices.[1,2] Since large amounts of optically active ions can be incorporated in these hosts, rare earth doped fluoride glasses have been widely studied for technological applications such as fiber, solid state lasers, three-dimensional (3D) displays and optical amplifiers,[1,2] for which higher quantum efficiencies from the excited levels are necessary.

Fluorozirconate glasses is one of the most important fluoride families, and large amount of the information about their 3D structure has been obtained from the comparative structural analysis of crystalline and devitrified [glass-ceramic (GC)] matrices.[3] It is generally accepted that the rare earth ion plays an important role in the stabilization of the glassy framework as a glass former in the fluorozirconate structures,[1,4–7] although Wang *et al.*[8] suggested, in ternary fluorozirconate glasses doped with Eu^{3+} and using x-ray absorption fine structure (XAFS), a glass intermediate behavior of the rare earth, being able to be in and out of the network positions. On the other hand, Ebendorff-Heidepriem *et al.*[9] in Ho^{3+}-doped fluorozirconate glasses and GCs emphasized the role of the Ho^{3+} as a glass stabilizer or as a heterogeneous nucleating agent depending upon the doping concentration.

For optical applications special interest is devoted to the analysis of the local structure around the rare earth ions in the matrix, since it rules the fine structure splitting of the free-ion multiplets and the forced intraconfigurational $4f$-$4f$ electric-dipole transitions probabilities in the optical range.[10] However, the exact nature of the local structure of the rare earth ions in the fluorozirconate glass is still unknown and the only information available is the existence of different environments due to the inherent disorder of the glass structure, which leads to site-to-site variations in the local bond distances and angles and, hence, to variations in the electronic energy levels of the rare earth ion. This feature gives rise to an inhomogeneous broadening of the absorption and luminescence spectral profiles.

Many techniques, such as NMR, x-ray diffraction, IR absorption or Raman spectroscopy, may give information on the structure of glasses, although they do not reflect the distribution and real symmetry of the environments of the rare

a)Author to whom correspondence should be addressed. Electronic mail: vlavin@ull.es.

earth ions. On the other hand, extended XAFS (EXAFS) and neutron scattering have been used to obtain information of the mean bond distances and the coordination numbers of the rare earth in glasses. However, the optical spectroscopy is the only one technique that allows studying the distribution of the environments for the optically active ions in glasses. For this purpose the Eu^{3+} ion has been usually used as a probe, mainly because of the large sensitivity of its luminescence on the local environment. The electronic energy level scheme of the Eu^{3+} ions in solids consists of seven ^7F_J $(J=0-6)$ multiplets well separated (around 12 000 cm^{-1}) from the ^5D_J $(J=0-4)$ ones and other strongly overlapped excited multiplets above the $^5D_3$ state at around 25 000 cm^{-1}. Thus the wave functions of the ^7F_J multiplets have an almost pure Russell-Saunders character (>95%).[11] Moreover, the luminescence takes place mainly in the visible range between the multiplets of the low-energy terms, ^7F and ^5D. However the most important and unique feature of the Eu^{3+} ions is the existence of crystal-field (CF) allowed $^7F_0 \leftrightarrow {}^5D_0$ transitions, i.e., transitions between singlet (nondegenerate) levels. Thus it is possible to selectively excite rare earth ions in a particular environment in which absorption energy is resonant with a laser light, provided that the laser spectral linewidth is much narrower than the inhomogeneous broadening. This technique is know as fluorescence line narrowing (FLN) and allows obtaining valuable information about the energy level structure, CF parameters, lifetimes, homogeneous linewidths, or energy transfer processes between Eu^{3+} ions in different environments in the glass.[12–14]

The FLN technique has been applied to the Eu^{3+}-doped fluorozirconate glasses,[5,15–19] although the subsequent analysis of the crystal field felt by the Eu^{3+} ions has been only limited to the $^7F_1$ multiplet and the site dependence of the second rank CF parameters $B_0{}^2$ and $B_2{}^2$. The emission to the other ^7F_J $(J=2-6)$ multiplets also show site-selective features, but the weak CFs found in this matrix, compared to oxide glasses,[20] and the inhomogeneous broadening of the different emission transitions to the ^7F_J Stark levels have complicated the analysis. The only attempt to include the $^7F_2$ multiplet in the CF study was developed by Harrison and Denning,[19] which using molecular dynamics have obtained the second and fourth rank CF parameters and have simulated the ^7F_J $(J=1,2)$ Stark energy level diagram.

From the FLN studies the rare earth ions are assumed to occupy well defined sites in the glassy framework.[1,4–7] However, in the past decade there has been a controversy about the number of sites or distribution of environments for the Eu^{3+} ions in fluoride glasses.[1] An interesting hypothesis was proposed by Adam *et al.*,[5] Lucas *et al.*,[6] and Poulain *et al.*[21,22] suggesting, from the direct comparison of the emission spectrum of the Eu^{3+}-doped fluorozirconate glass with that of the $EuZrF_7$ polycrystal, that this crystalline phase could be the parent structure that would explain the distribution of environments found for the Eu^{3+} ions in fluorozirconate glasses.

The aims of this work are obtaining a complete picture of the rare earth's local structures in the fluorozirconate glass and giving experimental evidences of the existence of a parent structure. However, these objectives cannot be reached with the as-made, or precursor, glass and different temperature and pressure-induced phase transition techniques have been applied on glassy and crystalline matrices monitoring the Eu^{3+} luminescence. These techniques will play a relevant role in the development of a structural model for the rare earth ions in the fluorozirconate glass.

In a first step, the Eu^{3+} luminescence in the fluorozirconate glass, the fluorozirconate GC and the $EuZrF_7$ polycrystal are presented and compared. In a second step, a CF analysis has been carried out for the Eu^{3+} ion in the GC. With the identification of those environments in the glass in which the Eu^{3+} ion felt a similar CF strength as in the GC, the CFs acting on the Eu^{3+} ions in the glass are calculated, thus allowing a suitable simulation of the ^7F_J $(J=0-6)$ Stark energy level diagram for the Eu^{3+} ions in the different environments present in the fluorozirconate glass. Finally, some conclusions about the local structure and the distribution of environments of the rare earth ion in the fluorozirconate glass are presented using a simple geometrical model.

II. EXPERIMENTAL

The heavy metal fluorozirconate glass starting composition (in mol %) was 50 ZrF_4-33 BaF_2-10 YF_3-7 AlF_3 and the doping concentration varied from 0.1 to 2.5 mol % of EuF_3. The mixture of raw materials was fluoridized in a covered vitreous carbon crucible at 420 °C for 45 min and melted at 850 °C for 45 min. Finally, the melt was poured into an open Al mold preheated to 260 °C. The differential scanning calorimetry measurement shows a $T_g=326$ °C and a $T_x=390$ °C (onset of the crystallization peak).

The fluorozirconate GC was obtained after a thermal treatment of the precursor glass at 390 °C for 3 h. For the GC doped with 2.5 mol % of Eu^{3+} under study, the β-$BaZrF_6$ crystalline phase has been observed by x-ray diffraction. Ebendorff-Hiedepriem *et al.*[9] found the same phase for the undoped fluorozirconate GC under study and its crystallization is favored by the increase in the rare earth doping concentration through an heterogeneous nucleation.

The $EuZrF_7$ polycrystal was obtained in three steps: a thermal treatment at 800 °C for 14 h in a sealed platinum crucible, followed by another one at 750 °C for 20 h and finally a rapid cooling of the crucible with cooled water. The x-ray diffraction analysis confirmed the existence of the monoclinic $EuZrF_7$ phase with the spatial group $P2_1$ and the same structural parameters as those originally obtained by Poulain *et al.*[23] In the $EuZrF_7$ crystalline phase, the EuF_8 and the ZrF_6 polyhedra make an infinite 3D framework containing large holes. The EuF_8 polyhedron of the Eu^{3+} ions is surrounded by five fluorine ions forming a near square pyramid while the other three ones form a nonregular triangle. This local environment is shown in Fig. 1(a).[23] and has only one near-mirror plane of symmetry, apart from the identity, which contains four fluorine ions. Thus, in this crystalline phase the Eu^{3+} local structure has a monoclinic structure with a nearly C_S point symmetry.

For site-selective FLN measurements a tunable dye laser (Lambda Physik) operating with rhodamine 6G, pumped by a *Q*-switched 532 nm frequency-doubled Nd:YAG (yttrium

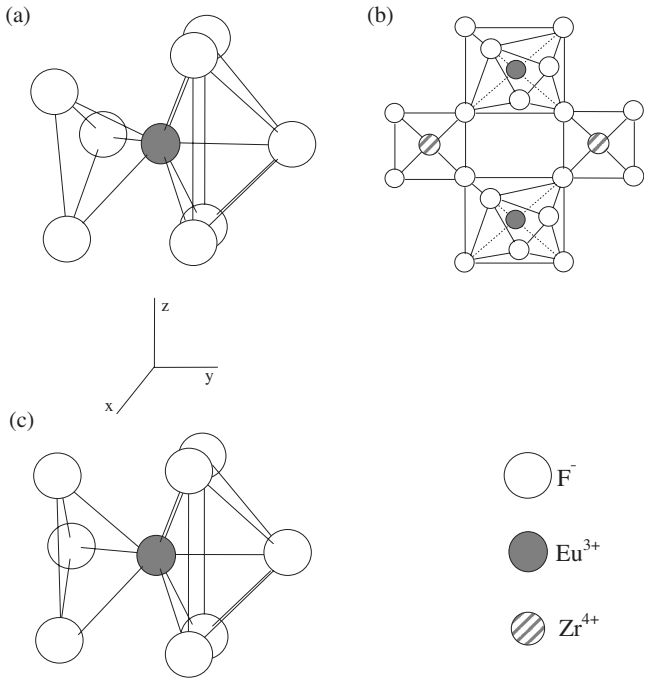

FIG. 1. (a) EuF_8 polyhedra in the $EuZrF_7$ crystalline phase and (b) idealized association of the EuF_8 and ZrF_6 polyhedra in a projection parallel to the mirror plane of symmetry (*y* view), after Poulain *et al.* (Ref. 23). (c) Idealized EuF_8 polyhedra used in the calculations. Displayed axis refers to the plots (a) and (c).

aluminum garnet) laser (Continuum Surelite-I), was used as excitation source. The laser spectral linewidth was 0.15 cm^{-1} and the pulse width was 5 ns with a repetition rate of 19 Hz. For time-resolved resonant FLN measurements within the $^5D_0$ level a phosphorimeter (Spex 1934C) connected to the *Q*-switching control of the Nd:YAG laser triggered the laser pulse while a synchronous mechanical chopper blocked the laser light from the luminescence signal that reach the detection system. High and low resolution luminescence spectra were detected through a 0.75 m single grating and a 0.22 m double-grating monochromators (Spex 750M and 1680), respectively, with a cooled photomultiplier tube (PMT) (Hamamatsu R943–02) operating in a photon counting technique (Spex DM302). Site-selective luminescence decays were recorded by sending the PMT signal directly to a digital storage oscilloscope (Tektronix 2430) equipped with different load resistors (0.1–10 kΩ) and controlled by a computer. Measurements were made at 13 K using a close-cycled helium cryostat (APD Corp.).

For room temperature (RT) high-pressure measurements up to 19.3 GPa the $EuZrF_7$ polycrystal was inserted in a miniature diamond anvil cell (mini-DAC) made at The University of Paderborn (Germany). Because of the hygroscopic nature of the matrix, water-free octane was used for the pressure transmitting medium, providing hydrostatic conditions in this range of pressures at RT,[24] and the pressure was determined by the ruby luminescence technique. The luminescence of the Eu^{3+} ions was excited by the 488 nm line of an Ar^+ laser (Innova 70) and recorded using a 1 m double-grating monochromator (Spex 14018) with a cooled PMT (Hamamatsu R943-02) operating in a photon counting technique (Hamamatsu C9744).

The IR spectrum was measured with a Fourier transform-IR spectrometer (Bruker), whereas the Raman spectra was detected with a double-additive spectrometer (Jobin Yvon U1000) and a high-sensitive charge coupled device detector (JY Symphony) using as excitation source the 514 nm line of an Ar^+ laser. All the spectra were corrected from instrument response.

III. THEORETICAL BACKGROUND

The optical properties and the energy level diagram of the rare earth (RE^{3+}) ions in solids are ruled by the interelectronic interaction between the electrons of the inner $4f$ shell of the RE^{3+} ion and the charge of the host ligands, all distributed in a particular local point symmetry. The complete Hamiltonian (free-ion plus CF interactions) describing the RE^{3+} ions in solids uses a parametric method, in which a small group of phenomenological parameters allow to reproduce the rare earth's energy level diagram. In the framework of the Racah algebra, the interaction is described by a sum of products of radial integrals by tensor operators. The angular components of the tensor operators can be calculated exactly with the help of the tensor algebra and the group theory,[10] while the radial integral are taken as adjustable numerical coefficients.

The free-ion Hamiltonian including interelectronic, spin-orbit, and many-body interactions is usually written as[10,25–27]

$$H_{\mathrm{FI}} = E_{\mathrm{av}} + \sum_{k=2,4,6} f_k F^k + \zeta_{ls} A_{ls} + \alpha l(l+1) + \beta G(G_2) + \gamma G(R_7) + \sum_{i=2,3,4,6,7,8} t_i T^i + \sum_{j=0,2,4} M^j m_j + \sum_{k=2,4,6} P^k p_k \tag{1}$$

giving rise to 19 phenomenological parameters plus the mean energy of the whole configuration.

The one-electron CF Hamiltonian, responsible of the Stark fine splitting of the $^{2S+1}L_J$ multiplets and the $4f$-$4f$ intraconfigurational optical transitions, can be written as a sum of products of the renormalized spherical tensor operators, $C_q^{(k)}$, and the real, B_q^k, and imaginary, $B_q'^k$, parts of CF parameters in the form[10]

$$H_{\mathrm{CF}} = \sum_{k=0}^{\leq 6} \sum_{q \geq -k}^{\leq k} B_q^k [C_{-q}^{(k)} + (-1)^q C_q^{(k)}] + i B_q'^k [C_{-q}^{(k)} - (-1)^q C_q^{(k)}], \tag{2}$$

where the values of k and q for which the parameters are nonzero are determined by the local symmetry.

Most of the intraconfigurational transitions between $4f$ states of the RE^{3+} ions are electric dipole in nature, whereas only a few of them show magnetic-dipole character and are nearly independent of the matrix. The Judd–Ofelt theory[28–30] considers that the electric-dipole absorption and emission transitions are forced by interconfigurational opposite-parity wave function mixing induced by the odd CF interaction generated by the ligands on the RE^{3+} ion site. Thus the $4f$-$4f$ electric-dipole absorption and emission probabilities can be

expressed in terms of three intensity or Judd–Ofelt parameters (Ω_2, Ω_4, and Ω_6) that characterize a RE^{3+} ion in a given matrix,[28–30]

$$\text{absorption} \propto f_{\text{ED}} = \frac{8\pi^2 m\nu}{3h(2J+1)} \frac{n(n^2+2)^2}{9} \sum_{\lambda=2,4,6} \Omega_\lambda \langle f^N \Psi J \| U^{(\lambda)} \| f^N \Psi' J' \rangle^2, \tag{3}$$

spontaneous emission:

$$A_{\text{ED}} = \frac{64\pi^4 \nu^3}{3h(2J+1)} \frac{n(n^2+2)^2}{9} \sum_{\lambda=2,4,6} \Omega_\lambda \langle f^N \Psi J \| U^{(\lambda)} \| f^N \Psi' J' \rangle^2, \tag{4}$$

where ν is the mean frequency of the transition, J is the angular momentum of the initial level, n is the refractive index, $\langle \| U^{(\lambda)} \| \rangle$ are the reduced matrix elements, which depend on the RE^{3+} ions but not on the host, and the Judd–Ofelt parameters can be expressed as

$$\Omega_\lambda = (2\lambda+1) \sum_{k,q} \frac{1}{2k+1} |A_{kq}|^2 \Xi^2(k,\lambda) \propto \sum_{k,q,l'} |A_{kq}|^2 \frac{\langle 4f|r|n'l'\rangle \langle n'l'|r^k|4f\rangle}{\Delta E(\Phi'')}, \tag{5}$$

where $\Xi(k,\lambda)$ includes monoelectronic radial integrals, energy difference between configurations, and $3j$ and $6j$ symbols that characterize the interconfigurational $(4f^N \leftrightarrow 4f^{N-1}n'l')$ interaction and the A_{kq}^{odd} are the odd ($k=3,5,7$) CF parameters ($B_q^k \propto r^k A_{kq}$) that depend on the nature, symmetry and strength of the ion-ligand interaction in the host.

The even part of the one-electron CF Hamiltonian, responsible of the CF splitting, can be written for the C_S symmetry, for which all the odd-q parameter vanishes, as[10]

$$\begin{aligned} H_{\text{CF}}^{(\text{even})}(C_s) = {} & B_0^2 C_0^{(2)} + B_2^2 (C_{-2}^{(2)} + C_2^{(2)}) + iB_2'^2 (C_{-2}^{(2)} - C_2^{(2)}) \\ & + B_0^4 C_0^{(4)} + B_2^4 (C_{-2}^{(4)} + C_2^{(4)}) + iB_2'^4 (C_{-2}^{(4)} \\ & - C_2^{(4)}) + B_4^4 (C_{-4}^{(4)} + C_4^{(4)}) + iB_4'^4 (C_{-4}^{(4)} - C_4^{(4)}) \\ & + B_0^6 C_0^{(4)} + B_2^6 (C_{-2}^{(6)} + C_2^{(6)}) + iB_2'^6 (C_{-2}^{(6)} \\ & - C_2^{(6)}) + B_4^6 (C_{-4}^{(6)} + C_4^{(6)}) + iB_4'^6 (C_{-4}^{(6)} - C_4^{(6)}) \\ & + B_6^6 (C_{-6}^{(6)} + C_6^{(6)}) + iB_6'^6 (C_{-6}^{(6)} - C_6^{(6)}), \end{aligned} \tag{6}$$

with 15 nonvanishing CF parameters (9 real and 6 imaginary). One of them could be selected as zero by a suitable rotation around the central RE^{3+} ion. Furthermore, since there is no principal axis for the C_S symmetry, the z-axis can be arbitrarily selected and different sets of CF parameters (that could give the same CF splitting) can be obtained without any clear link between them.[31] This fact makes necessary to give the set of axis used in the CF description and then use the transformations proposed by Rudowicz and Bramsley[32] in order to compare the results obtained with different coordinates of symmetry.

However, in the description of the CF interaction is useful to define a scalar, rotationally invariant parameter known as the scalar CF strength parameter. According to those developed by Auzel and co-worker[33,34] and Leavitt,[35] the scalar CF strength parameter used here is

$$S = \left[\sum_k (S^{(k)})^2 \right]^{1/2} = \left[\sum_k \frac{1}{2k+1} \frac{1}{3} \left\{ |B_0^k|^2 + 2 \sum_{\substack{q \le k \\ q>0}} (|B_q^k|^2 + |B_q'^k|^2) \right\} \right]^{1/2}. \tag{7}$$

This definition allows obtaining relative percentage values of the influence on several k rank contributions in the S value, defined as

$$\%S^{(k)} = 100 \left(\frac{S^{(k)}}{S} \right)^2. \tag{8}$$

In order to start the simulation of the CF interaction in the fluoride hosts under study, an initial estimation of the CF parameters have to be obtained using the crystalline structure of the $EuZrF_7$ crystal, as will be explained later. For this purpose, *ab initio* calculations have been developed making use of the very simplified simple overlap model (SOM),[36] which uses only the first neighbors around the RE^{3+} ion, to provide starting parameters given by

$$B_q^k = \rho \left(\frac{2}{1 \pm \rho} \right)^{2k+1} \langle r^k \rangle A_q^k \tag{9}$$

where the minus sign indicates covalent bonding character, ρ is the overlap between orbitals being the only one additional parameter that, in a first approach, is assumed to have a value of 0.05 for the Eu^{3+} ion,[36] $\langle r^k \rangle$ are the radial integrals of the RE^{3+} ion, for which the Freeman–Watson values are taken,[37] and the RE^{3+} local site symmetry is taken into account through the lattice sum, A_q^k, given by

$$A_q^k = \sqrt{\frac{4\pi}{2k+1}} \sum_j \frac{g_j}{R_j^{k+1}} Y_q^{k*}(j) \tag{10}$$

being g_j the charge of ligands (F^- ions) and R_j its distance from the central Eu^{3+} ion.

The SOM model have been selected to obtain the *ab initio* CF parameters since in vitreous structures there are strong distortions or deformations in the 3D structure at long distances but one may expect weak local distortion for a constitutional ion. This local calculation, disregarding the long range vitreous deformations, appears as a good starting point to this kind of analysis. Unfortunately, and because of the approximated C_S local symmetry, it is not possible to construct an *ab initio* set of CF parameters in which most of the odd-q CF parameters vanishes using the crystallographic data reported by Poulain *et al.*[23] Thus it is necessary to work with an idealized structure for the RE^{3+} local environment.

TABLE I. Different sets of CF parameters and ^7F_J barycenters in a fluorozirconate GC (in cm^{-1}). The *ab initio* calculation uses the SOM within the first coordination shell of the Eu^{3+} ion in the $EuZrF_7$ crystal. Calculated sets A and B only differ in the values of the nonaxial CF parameters of rank 6 to give the same Stark energy level fitting, while small changes in those parameters of ranks 2 and 4 are consequence of the compensation of this change (see text).

		Calculated	
CF Parameters	*Ab initio* (SOM)	A	B
B_0^2	−132	**−54**	**−85**
B_2^2	−162	**−298**	**−275**
B_0^4	−808	**−996**	**−941**
B_2^4	502	**−193**	**−301**
$B_2'^4$	494	**515**	**550**
B_4^4	−100	**317**	**395**
$B_4'^4$	−179	**−5**	**−82**
B_0^6	−229	**−118**	**−120**
B_2^6	−82	−387	139
$B_2'^6$	−319	120	282
B_4^6	−166	141	−177
$B_4'^6$	−388	−110	58
B_6^6	−209	−189	14
$B_6'^6$	262	207	−155
Barycenters			
$^7F_0$		24	23
$^7F_1$		401	401
$^7F_2$		1073	1074
$^7F_3$		1937	1934
$^7F_4$		2903	2901
$^7F_5$		3934	3935
$^7F_6$		5011	5009
CF strength			
S	301	306	305
$\%S^{(2)}$	5%	13%	11%
$\%S^{(4)}$	71%	71%	80%
$\%S^{(6)}$	24%	16%	9%
rms		6.5	5.9

The idealized structure, shown in Figs. 1(b) and 1(c), is constructed by maintaining the mean Eu^{3+}–F^- distances but using a true square straight pyramid in the right side of the Eu^{3+} ion and turning equilateral, and parallel to the square plane, the triangle depicted in the left side of the Eu^{3+} ion. From the several sets of parameters resulting from the different elections of the z-axis and from the transformations proposed by Rudowicz and Bramsley,[32] we have finally selected as starting parameters those obtained with the z-axis depicted in Fig. 1, in which the value of most q-odd parameters are zero (only B_1^6 and $B_1'^6$ have small nonzero values). Additionally, the axis set depicted in this figure is selected in such a way that the $B_2'^2$ parameter vanishes. The *ab initio* set of CF parameters obtained from the SOM model for this "idealized" structure is reported in Table I.

The fitting procedure that minimizes the sum of square residuals between the observed and the calculated Stark energy levels was achieved by using both the RECFCALC program developed by Muñoz-Santiuste[38] and the CFIT program developed by Reid (University of Canterbury, New Zealand).

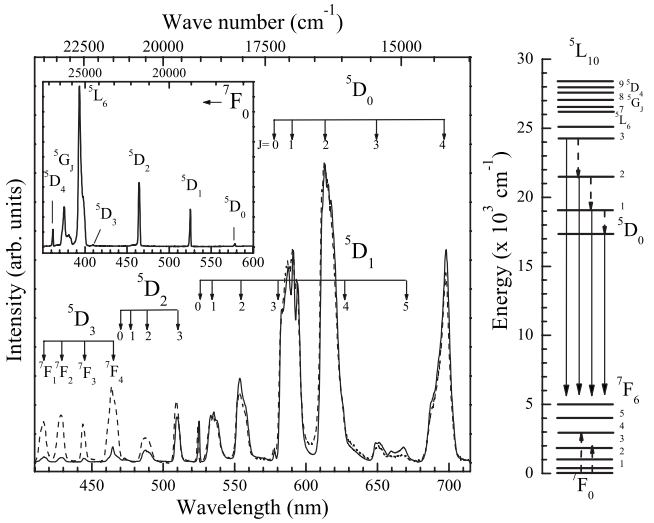

FIG. 2. Emission spectra in fluorozirconate glasses doped with 0.1 (---) and 2.5 (—) mol % of Eu^{3+} ions exciting the $^7F_0 \rightarrow {}^5L_6$ transition at 395 nm at 13 K. Transitions start from the ^5D_J (J=0–3) levels to the indicated ^7F_J (J=0–6) levels. The $^5D_0 \rightarrow {}^7F_J$ (J=5,6) transitions although observed are not included. The inset figure shows the excitation spectrum in a fluorozirconate glass doped with 2.5 mol % of Eu^{3+} ions monitoring the $^5D_0 \rightarrow {}^7F_2$ transition at 612 nm at 13 K. Transitions start from the $^7F_0$ ground state to the indicated levels. The spectral resolution is 0.2 nm. Partial free-Eu^{3+} ion energy level diagram is also included and the radiative emissions (solid) and nonradiative cross-relaxation channels (dashed) are shown.

IV. LUMINESCENCE

A. Fluorozirconate glass

The excitation and emission spectra of the Eu^{3+} ions in fluorozirconate glasses doped with 0.1 and 2.5 mol % of Eu^{3+} ions, obtained under broadband conditions at 13 K, are given in Fig. 2. They consist in a set of inhomogeneously broadened bands due to the diversity of local environments occupied by the RE^{3+} ion in the glass. Each band is associated to a transition between different $^{2S+1}L_J$ multiplets within the $4f^6$ ground configuration and has been identified straightforwardly comparing the peak energies with the free-Eu^{3+} ion energy level diagram (see Fig. 2).[10,11,39]

The excitation spectrum is quite similar to the absorption one for both concentrations of Eu^{3+} ions. At low temperature the thermalization effect is negligible and all the absorption bands observed correspond to transitions starting from the $^7F_0$ ground level to the excited multiplets. On the other hand, the de-excitation of the RE^{3+} ions in low-phonon energy matrices, such as the fluorides, after the excitation to the upper excited states above 25 000 cm^{-1} results in a competition between visible (blue to orange) luminescence from the ^5D_J (J=1–3) multiplets and nonradiative de-excitations. The latter includes multiphonon de-excitation due to the RE^{3+}-ligands dynamic coupling and the concentration-dependent RE^{3+}-RE^{3+} energy transfer relaxations starting from the $^5D_3$ and $^5D_2$ levels to the lower lying $^5D_1$ and $^5D_0$ ones.[40] The effect of concentration quenching can be clearly observed in the differences of emission intensities from the upper emitting levels in fluorozirconate glasses doped with 0.1 and 2.5 mol % of Eu^{3+} ions (see Fig. 2). This feature is due to cross-relaxation processes involving the $^5D_3$ and $^5D_2$

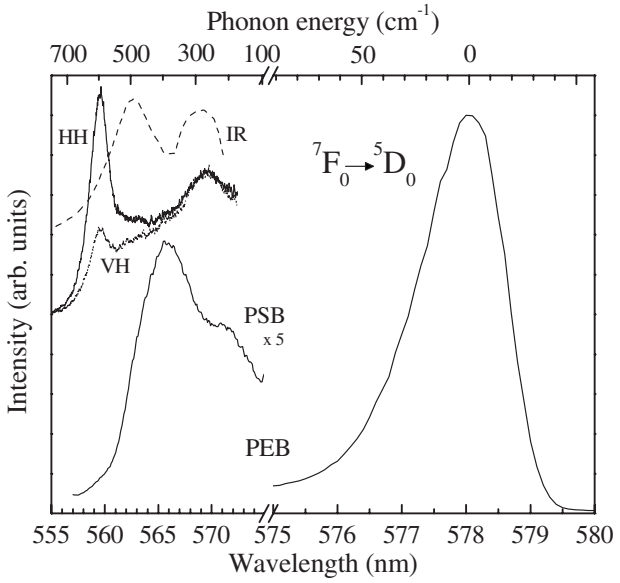

FIG. 3. $^7F_0 \rightarrow {}^5D_0$ excitation spectra in a fluorozirconate glass doped with 2.5 mol % of Eu^{3+} ions detecting the $^5D_0 \rightarrow {}^7F_2$ emission at 612 nm at 13 K. The high-energy band is a one-phonon vibronic or PSB associated to the PEB. The spectral resolution is 0.15 cm^{-1}. The IR and Raman spectra are given for comparison.

with the $^7F_0$ ground level. The most efficient cross-relaxation channels are given in the Eu^{3+} energy level diagram in Fig. 2.

From the $^5D_0$ nondegenerated level the Eu^{3+} ions decay radiatively to the ^7F_J (J=0–6) levels with a quantum efficiency of unity in the visible (yellow to red) and near IR range, since the large energy gap between the ^7F_J and the ^5D_J multiplets ($\sim$12 000 cm^{-1}) and the maximum phonon energies found in this sample ($\sim$500 cm^{-1}) make the probability of multiphonon de-excitation practically zero and, on the other hand, no cross-relaxation channels exist. The $^5D_0 \rightarrow {}^7F_1$ is a magnetic-dipole transition allowed by the selection rules and is almost independent of the matrix, if the J-mixing effect is negligible.[41] The $^5D_0 \rightarrow {}^7F_J$ (J=2,4,6) transitions are electric-dipole in nature and are forced by the odd CF Hamiltonian. The transition to the $^7F_2$ multiplet depends only on the Ω_2 Judd–Ofelt parameter and it shows a high degree of sensitivity to the nature and geometrical arrangement of the RE^{3+} local structure, being one of those called hypersensitive transition. The transition to the $^7F_4$ multiplet depends on Ω_4 while that to the $^7F_6$ multiplet on Ω_6. The other emission transitions, $^5D_0 \rightarrow {}^7F_J$ (J=0,3,5), are strictly forbidden in the frame of the intermediate scheme of the Judd–Ofelt theory,[29,30] and their low intensities are explained by the J-mixing effect that induces an effective borrowing of intensity from the other CF-forced electric-dipole transitions.[41–43]

In order to obtain information about the local structure of the Eu^{3+} ions in the fluorozirconate glass applying the FLN technique, special attention is paid to the transition between the nondegenerate levels, i.e., the $^7F_0 \rightarrow {}^5D_0$ transition. The excitation spectrum of this transition, shown in Fig. 3, is composed of a pure electronic band (PEB) centered at 578 nm and a high-energy lying vibronic or phonon sideband (PSB). The former involves pure electronic transitions between the $^7F_0$ ground state and the $^5D_0$ excited level of the Eu^{3+} ions in different local environments. The large full width at half maximum of this band is a consequence of the overlapping of the homogeneous spectra of the Eu^{3+} in each CF environment, which show slightly different transition energies. However, in fluoride glasses there is a narrower distribution of environments for the RE^{3+} ion compared to oxyfluoride and oxide glasses.[20] As will be shown later, the higher the energy of the $^7F_0 \rightarrow {}^5D_0$ homogeneous transition the stronger the CF interaction felt by the Eu^{3+} ions.

The vibronic band involves simultaneous vibrational and electronic transitions, and will give more precise information about the nature and energies of the phonons involved in the RE^{3+} local structure than the IR and Raman spectra. Since the probability of multiphonon excitation is rather low compared to the excitation of one phonon, in this transition only participate single phonons of the glass.[15,19,41,44–46] Moreover, according to the Judd approach for the vibronically induced forced electric-dipole transition,[47] the intensity of the PSB shows a R^{-6} dependence on the rare earth to ligand distance, indicating that the PSBs observed in Fig. 3 are dominated by the ligand ions forming the immediate environment of the Eu^{3+} ions. Thus the energy shift of the PSB related to the PEB gives a direct measurement of the energy of the phonons involved in the Eu^{3+} local structures.

It is worth noting that the phonon energies obtained by the PSB spectrum are smaller than those found by vibrational Raman and IR spectroscopies (see Fig. 3), indicating that there are some differences in the phonon energies involved in the Eu^{3+} local structure and those of the glass network. This feature was explained by Todoroki *et al.*[48] using a simple coupled oscillation model and taking into account that the Raman- and IR-active phonon modes correspond to the stretching vibrational energy of the strongest bonding in the glass matrix, i.e., the vibration of the framework of the glass, whereas the phonons obtained through the PSB spectrum are due to the local vibration coupled with the electrons of the RE^{3+} ion.

It is generally accepted that the minor components of the glass, i.e., AlF_3 and YF_3, have small or negligible effects on the vibrational IR and Raman spectra when present in small concentration,[49] although their presence is important in other aspects since they favor the decrease in the crystallization rate, the increase in the glass stability and the compactness of the glass, occupying sites usually empty in the basic glass.[6,7] Thus the IR and Raman spectra obtained for the ZrF_4-based glass under study can be compared to those obtained for binary barium fluorozirconate glasses.[50] In these glasses the large Ba^{2+} ions breaks the periodicity of the structure, modifying the glass network and generating a great variety of polyhedra with extremely variable Zr–F–Zr angles. Thus the vitreous network is constructed from the association of ZrF_6, ZrF_7, and ZrF_8 polyhedra sharing corners or edges, which complicate the vibrational spectra. However, Almeida[49] placed forward a pair of tentative empirical selection rules for the main Raman- and IR-active modes of fluorozirconate glasses: The Raman spectrum is dominated by high frequency symmetric stretching vibrations of nonbridging fluorine atoms around fixed network forming cation, whereas the

IR spectrum is dominated by stretching vibrations of bridging fluorine atoms accompanied by a small amount of network forming cation motion. Following these rules, the 600 cm^{-1} Raman-active mode can be assigned to the symmetric stretching of nonbridging fluorines without Zr cation motion, the 500 cm^{-1} IR-active mode is the antisymmetric stretch of bridging fluorines with simultaneous Zr cation motion and the 275 cm^{-1} IR-active is the symmetric stretch of bridging fluorines with Zr motion.[49]

Taking into account the previous arguments, the peaks of the PSB spectrum can be associated to the symmetric and antisymmetric motions of the nonbridging and bridging fluorine atoms of the different $Eu^{3+}-F^{-}-Zr^{4+}$ vibrational modes in the glass network,[25] although it seems that there is a preference of the Eu^{3+} ions to link with bridging fluorine ions. This result seems to be in good agreement with the idea that the RE^{3+} ion may act as a network forming and network modifying ion of the glass[6,7] and, together with the higher ionicity RE^{3+}-F^{-} bonds and a weaker polymerized network of this glass, would explain the small distribution of environments for the RE^{3+} ion, showing a higher regularity with only slightly different bond distances and angles that can be pictured by the short linewidth of the $^7F_0 \rightarrow {}^5D_0$ PEB. In this highly ionic glass the Eu^{3+} ion may have environments having coordination number ranging from 7 to 9 owing to the smaller radius of the F^{-} ion and inducing large RE^{3+}-F^{-} ionic ratios,[51] although using molecular dynamic simulation and EXAFS measurements it has been stated that the eight-coordinated environments seems to be predominant.[19,52]

In order to isolate the emission of the $^5D_0$ level from that of the $^5D_1$ level, the laser excitation was tuned at 565 nm at the maximum of the PSB.[15,19] The emission bands obtained, associated to the $^5D_0 \rightarrow {}^7F_J$ $(J=0-6)$ transitions, are inhomogeneously broadened due to a nonselective excitation process, as will be discussed later. The broadband spectrum for a fluorozirconate glass doped with 2.5 mol % of Eu^{3+} ions is partially depicted at the bottom of Figs. 4 and 5. The presence of three peaks for the $^5D_0 \rightarrow {}^7F_1$ transitions is the first indication of the low symmetry of the Eu^{3+} environments in the fluorozirconate glass, for which the (even) CF interaction totally removes the degeneracy of the $^7F_1$ multiplet. Moreover, the linewidths of the transitions, specially that of the $^5D_0 \rightarrow {}^7F_1$ one, again show a relative narrower distribution of environments for the Eu^{3+} ions in the fluoride glass compared to those in oxide glasses.[20,41]

The existence of a variety of local structures for the Eu^{3+} ions in the fluorozirconate glass becomes evident after applying the FLN technique exciting selectively with laser light within the $^7F_0 \rightarrow {}^5D_0$ PEB. The site-selective emission spectra of the $^5D_0 \rightarrow {}^7F_J$ $(J=1-5)$ transitions are shown in Figs. 4 and 5 for some selected excitation wavelengths in the fluorozirconate glass doped with 2.5 mol % of Eu^{3+} ions. It is worth noting the great sensitivity of the emissions of the Eu^{3+} with the environment that, since the emitting level is nondegenerated, can be associated to the a smooth change of the ^7F_J Stark splitting with the CF strength.[5,13,16–20,41] Although a better resolution is generally found, the inhomogeneous broadening is still important, specially for the emissions to the ^7F_J $(J=2-6)$ multiplets.

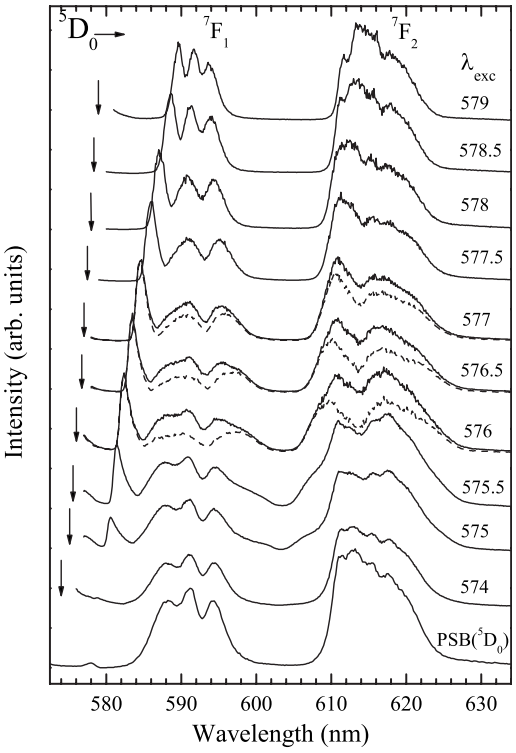

FIG. 4. FLN emission spectra to the ^7F_J $(J=1,2)$ multiplets exciting selectively the $^5D_0$ level in a fluorozirconate glass doped with 2.5 mol % of Eu^{3+} ions at 13 K. Excitation wavelength is indicated for each spectrum (in nm) and with vertical arrows. The lower spectrum corresponds to the broad band emission obtained after exciting at 565 nm the PSB coupled to the $^5D_0$ level at 13 K. Dotted lines indicate the spectra resulting from the subtraction of the broad band contribution. The spectral resolution is 0.2 nm.

As shown in Fig. 4, for excitation wavelengths above 577 nm three peaks are observed for the $^5D_0 \rightarrow {}^7F_1$ transition, indicating the existence of CF environments of low point symmetry, whereas for lower excitation wavelengths, in the range from 576 to 577 nm, some extra peaks are observed, which rapidly increases their intensities to reproduce the inhomogeneously broadened emission when the excitation reaches the high-energy side of the PEB. The interpretation of these site-selective spectra is still a matter of discussion. Some researchers[5,16,17] have considered the existence of the extra peaks as due to the presence of two main sites for the Eu^{3+} ions in fluoride glasses that contribute to the $^5D_0 \rightarrow {}^7F_1$ emission. Balda *et al.*[16] supported this hypothesis after the observation, using a pulsed excitation, of a resonant emission together with an energy transfer-induced nonresonant emission of Eu^{3+} ions in different environments in ZrF_4- and InF_3-based fluoride glasses.

In order to analyze this possibility in the glass under study, the time-resolved $^5D_0 \rightarrow {}^7F_0$ luminescence of the Eu^{3+} ions in one of the strongest CF environments in the glass has been studied after a laser pulse at 576 nm. As shown in Fig. 6, the resonant emission peak is accompanied by a broad inhomogeneous emission band, whose relative intensity is independent of the delay after the laser pulse. Moreover, the inset in this figure gives the emission to the $^7F_1$ multiplet for low-doped samples (0.1 and 1 mol % Eu^{3+}), in which more than three peaks are clearly observed, even though one can disregard energy transfer processes in the lowest concentra-

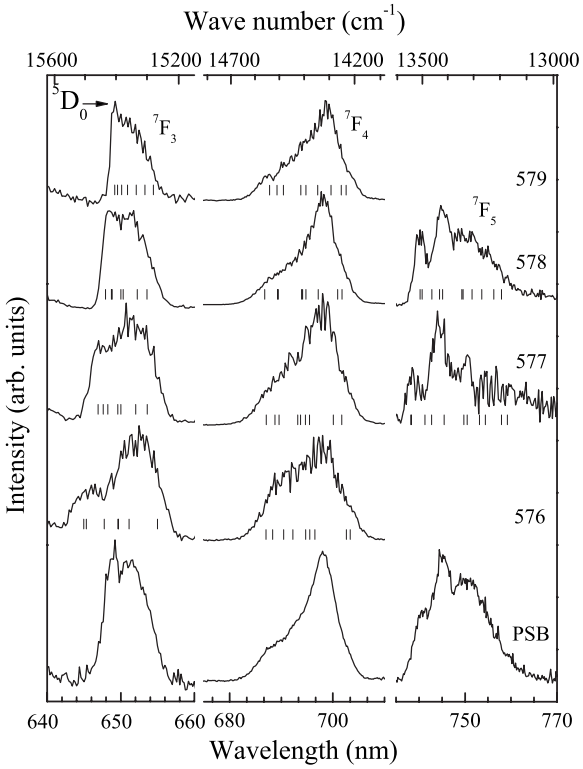

FIG. 5. FLN emission spectra to the ${}^7F_J$ ($J=3-5$) multiplets exciting selectively the ${}^5D_0$ level in a fluorozirconate glass doped with 2.5 mol % of Eu^{3+} ions at 13 K. The emission bands are normalized and the spectral resolution is 0.2 nm. The calculated energies of the emissions to the different Stark components of the ${}^7F_J$ multiplets are included (see text).

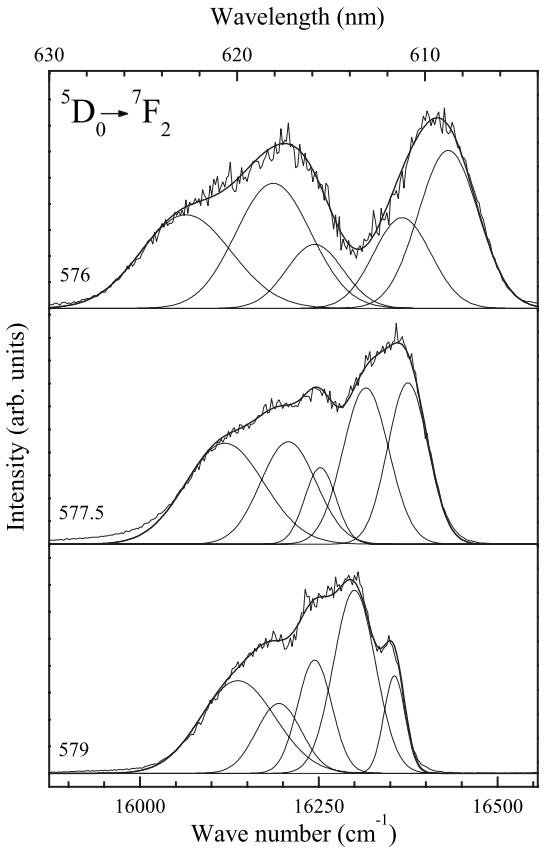

FIG. 7. Gaussian deconvolution of the ${}^5D_0 \rightarrow {}^7F_2$ emission profiles at different ${}^5D_0$ excitation wavelengths. The sum of the five Gaussian functions for each excitation wavelength is also given.

tion sample. These results indicate that these extra peaks are due to a simultaneous excitation of all the Eu^{3+} ions in the glass through the excitation of a broad, highly overlapped low-energy PSB associated to the ${}^5D_0$ level, rather than to the existence of more than one kind of site. The spectra obtained exciting below 576 nm show a progressive loose in the degree of selectivity when the PEB and the PSB are simultaneously excited, in agreement with the results found by Harrison and Denning[19] for ZBLAN glasses. Moreover, the complete loose in the selectivity is achieved for excitation wavelengths below 574 nm, resulting in a broad emission spectrum due to Eu^{3+} ions in the whole distribution of environments (see Figs. 4 and 5) due to the highly overlapped PSBs of the Eu^{3+} ion in each environment.[19]

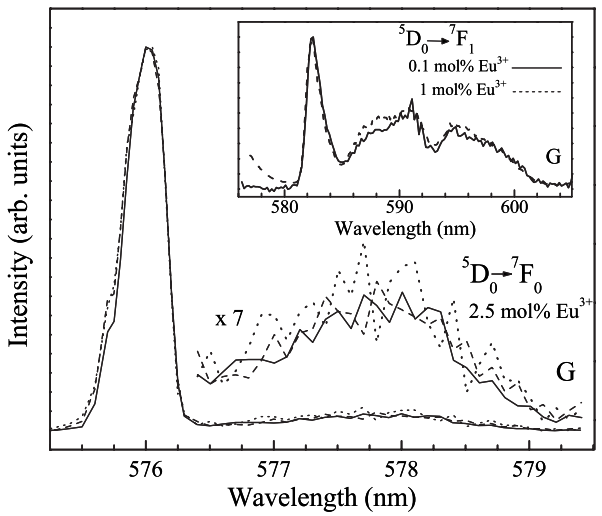

FIG. 6. Time-resolved FLN spectra of the ${}^5D_0 \rightarrow {}^7F_0$ transition in a fluorozirconate glass doped with 2.5 mol % of Eu^{3+} ions obtained 0.5 (—), 5 (---), and 9 ms (·····) after the laser pulse at 576 nm at 13 K. Spectra are normalized to the maximum of the resonant emission. Inset figure gives the ${}^5D_0 \rightarrow {}^7F_1$ emission spectra in fluorozirconate glasses doped with 0.1 and 1 mol % of Eu^{3+} ions exciting at 576 nm at 13 K. The spectral resolution is 0.2 nm.

For the CF calculation and energy level simulation, which will be discussed later, it is important to determine the real positions of the ${}^5D_0 \rightarrow {}^7F_J$ peaks of the Eu^{3+} ions resonantly excited between 576 and 577 nm. In the case of the three ${}^7F_1$ Stark levels, they can be directly obtained after subtracting the inhomogeneous contribution from the FLN emission spectra (see Fig. 4). The process for the five ${}^7F_2$ Stark levels needs also a Gaussian deconvolution of the band profile after the inhomogeneous subtraction, as shown in Fig. 7 for different ${}^5D_0$ excitation wavelengths. For this purpose it has been followed the criteria used by Brecher and Riseberg,[13] which takes into account that progressive changes in the energy positions and relative intensities have been assumed in the deconvolution process of the ${}^5D_0 \rightarrow {}^7F_2$ emission spectra since there are neither crossing between components nor relevant changes in their intensities from each spectrum to the following one, as already suggested from the FLN spectra (see Figs. 4 and 5). However, even these criteria fail when trying to deconvolute the

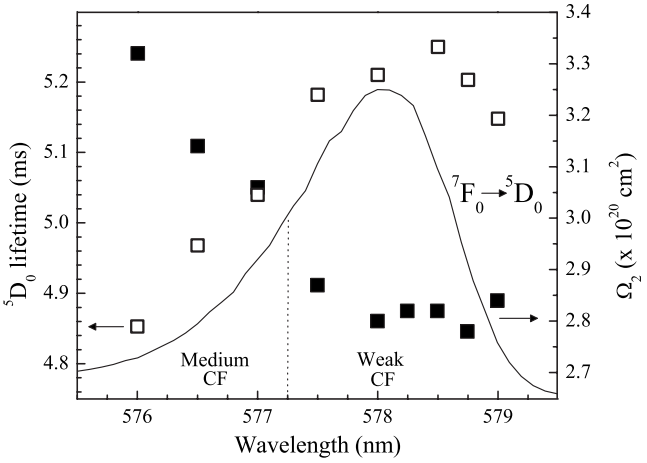

FIG. 8. The lifetime τ (□) of the $^5D_0$ emitting level and the Ω_2 (■) Judd–Ofelt intensity parameter as a function of the excitation wavelength within the $^7F_0 \rightarrow {}^5D_0$ excitation band (also shown).

$^5D_0 \rightarrow {}^7F_J$ $(J=3-6)$ emission bands due to the large inhomogeneous broadening, observed even after applying the FLN technique.

As a consequence of this broadening, most of the CF studies in fluoride matrices have been focused only on the $^7F_1$ Stark levels to calculate the B_q^2 CF parameters.[5,15–19] Comparing the real splitting of the $^7F_1$ multiplet and the second rank CF parameters found for the Eu^{3+} ions in the fluorozirconate glass with those found in oxyfluoride or oxide glasses,[20,41] there are no strong CF environments in the fluorozirconate glass as can be generally pure or mixed oxide glasses. Thus, a rough division between Eu^{3+} ions occupying weak and medium CF strength environments can be given in the studied fluoride glass. The border between the weak and the medium CF strength environments, shown in Fig. 8, is not strict and has been taken as that in which the *J*-mixing effect,[10] that mixes the wave functions of the closer $^7F_1$ and $^7F_2$ Stark levels, becomes increasingly important.

On the other hand, there is also an increase of the odd CF interaction in medium CF environments that will result in changes in the absorption and emission probabilities of the Eu^{3+} ion. This feature can be monitored measuring the lifetime of the $^5D_0$ level for the different environments, exciting selectively the optically active ions in the fluorozirconate glass doped with 2.5 mol % of Eu^{3+} ions. In order to assure the site selectivity in these measurements when exciting in the high-energy side of the $^5D_0$ level, the emission corresponding to the high-energy component of the $^5D_0 \rightarrow {}^7F_1$ transition was monitored. The results, shown in Fig. 8, show a monotonic decrease from around 5.25 ms to around 4.85 ms with the increase in the CF strength, whereas a mean value of 5.2 ms was obtained under broadband excitation.

In order to correlate the values of the lifetime with the different local environments of the Eu^{3+} ions in the fluoride glass, it is worth noting that the $4f$-$4f$ intensity probabilities of the RE^{3+} ions depend on the odd CF parameters squared [Eqs. (3)–(5)], whereas the splitting of the multiplets changes linearly with the even CF parameters [Eq. (7)]. Thus the intensities of the emission peaks are potentially more sensitive to variations in the local structure of the Eu^{3+} environments than the peak positions. Since the Eu^{3+} emission from the $^5D_0$ level is purely radiative, and neglecting the migration of energy between Eu^{3+} ions,[53] the change shown by the lifetime, and hence by the emission probability $(A=1/\tau)$, of the Eu^{3+} ions in different local structures has to be ascribed mainly to changes in the probabilities of the $^5D_0 \rightarrow {}^7F_J$ emissions.

The $^5D_0 \rightarrow {}^7F_1$ magnetic-dipole transition is nearly independent of the host matrix and the electric-dipole $^5D_0 \rightarrow {}^7F_J$ $(J=3-6)$ emissions scarcely show appreciable changes in their intensities. Thus the main changes in the emission probability has to be ascribed to the CF-induced electric-dipole $^5D_0 \rightarrow {}^7F_2$ hypersensitive transition, which only depends on Ω_2 and is very sensitive to the local structural changes in the vicinity of the optically active ions.[54] A usual measurement of how close the environment of the Eu^{3+} ion is to a centrosymmetric symmetry, or as a degree of the local structural distortion around the RE^{3+} ion, is the electric $^5D_0 \rightarrow {}^7F_2$ to the magnetic $^5D_0 \rightarrow {}^7F_1$ intensity ratio,[55] since the odd CF Hamiltonian is zero for this symmetry. The ratio of the $^5D_0 \rightarrow {}^7F_2$ and $^5D_0 \rightarrow {}^7F_1$ emission intensities reveals an almost constant value for the weak CF environments and an enhancement of the electric-dipole transition from weak to medium CF environments, which can be related to the increasing asymmetry of the geometrical local structure surrounding the Eu^{3+} ions in the fluorozirconate glass.[53]

It can be concluded that the change in the lifetime from roughly 5.25 ms in weak CF environments to 4.85 ms in medium CF environments is associated to variations in the probability of the $^5D_0 \rightarrow {}^7F_2$ transition, which can be directly correlated with variations in Ω_2 local structure hypersensitive parameter. From the site-selective radiative lifetimes and the branching ratios (relative areas of the emission peaks) obtained from the FLN spectra, the $^5D_0 \rightarrow {}^7F_2$ emission probabilities have been calculated for the different Eu^{3+} environments and, using Eq. (4), the Ω_2 parameter, which is shown as a function of the excitation wavelength in Fig. 8.

All these results support the hypothesis of an increasing distortion of the fluoride atoms polyhedron surrounding the Eu^{3+} ions when probing the weak and medium CF environments with the laser excitation energy, while from the FLN results it also seems that there is a unique class of site for all the distribution of environments present in the fluorozirconate glass. Unfortunately, no clear conclusions can be drawn about the real geometrical local structure of the environments occupied by the Eu^{3+} ions in the glass.

B. Temperature-induced glass-to-crystal phase transition

If a suitable picture of the RE^{3+} ion's local structures in the fluorozirconate glass wants to be given, a different strategy must be used, i.e., the analysis of the crystal structure of phases directly obtained after devitrifying or recrystallizing the fluorozirconate glasses. This technique takes advantage of the structural analogies found between the precursor glass and the subsequently devitrified matrix and has been used in the study of fluoride matrices.[3] This devitrified matrix, known as GC, consists of one glassy phase and one crystal

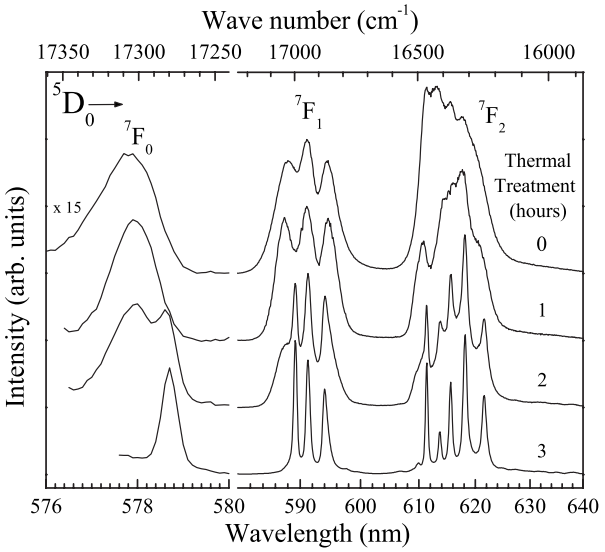

FIG. 9. $^5D_0 \rightarrow {}^7F_J$ ($J=0-2$) emission spectra in a fluorozirconate glass doped with 2.5 mol% of Eu^{3+} ions at 13 K after different thermal treatments at 390 °C (indicated in hours). The spectral resolution is 0.2 nm.

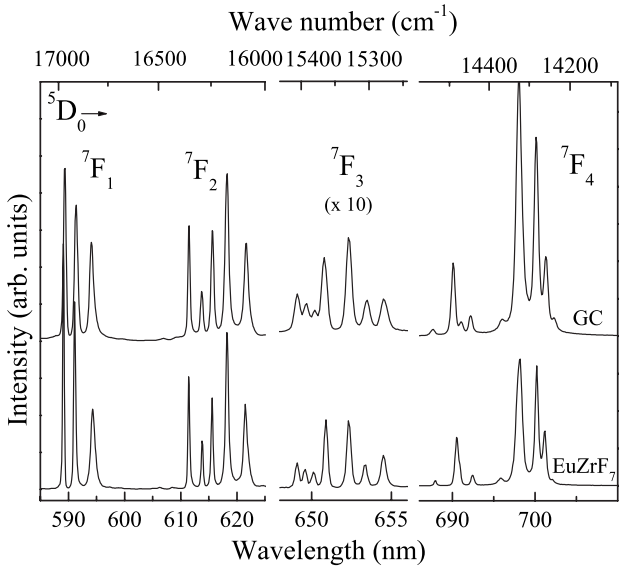

FIG. 10. $^5D_0 \rightarrow {}^7F_J$ ($J=1-4$) emission spectra in a fluorozirconate GC doped with 2.5 mol % of Eu^{3+} ions and in an $EuZrF_7$ polycrystal at 13 K. The spectral resolution is 0.05 nm.

phase and it is processed by a controlled nucleation and crystallization of the crystal phase in the precursor glass by a thermal process. In this temperature-induced phase transition the changes in the Eu^{3+} environment can be monitored by the changes in its optical properties.

The $^5D_0 \rightarrow {}^7F_J$ ($J=0-2$) emission spectra of the Eu^{3+} ions have been obtained for different times of thermal treatment at 390 °C, close to the crystallization temperature, of the fluorozirconate glass doped with 2.5 mol % of Eu^{3+} ions, (see Fig. 9). After 3 h of thermal treatment, the inhomogeneously broadened $^5D_0 \rightarrow {}^7F_0$ band of the Eu^{3+} ion in the fluorozirconate precursor glass is progressively transformed to a single sharp peak in the GC centered at 578.75 nm, typical of Eu^{3+} ions incorporated in a crystalline structure. This phase transition can be also followed with the line profiles of the $^5D_0 \rightarrow {}^7F_J$ ($J=1,2$) transitions that also suffer the same change, from broad bands to sharp peaks. Moreover, six groups of lines associated to the transitions to the ^7F_J ($J=1-6$) multiplets are clearly observed after the thermal treatment (see Figs. 10 and 11). Three sharp peaks for the $^5D_0 \rightarrow {}^7F_1$ emission transition, five for the $^5D_0 \rightarrow {}^7F_2$, seven for the $^5D_0 \rightarrow {}^7F_3$, and nine for the $^5D_0 \rightarrow {}^7F_4$ are depicted in Fig. 10. Only ten peaks can be clearly identified for the low intensity $^5D_0 \rightarrow {}^7F_J$ ($J=5,6$) transitions, shown in Fig. 11. The glassy-to-crystalline phase transition is also observed in the excitation spectra of the $^7F_0 \rightarrow {}^5D_J$ ($J=0-2$) transitions, for which one, three, and five peaks are observed (see Figs. 11 and 12).

Since the $^5D_0$ and the $^7F_0$ levels are nondegenerate, all these peaks are associated to transitions to the $2J+1$ Stark levels of each ^7F_J and ^5D_J multiplet, indicating that the degeneracy of the Eu^{3+} free-ion states is completely removed by the CF interaction in this crystalline phase. Moreover, almost all the Eu^{3+} ions enter in this ordered phase, since the emission at RT of the GC (not shown) only shows a rather weak broad shoulder at the high-energy side of the $^5D_0 \rightarrow {}^7F_0$ transition that indicates a minimal residual amount of Eu^{3+} ions in the glassy phase.

In order to obtain information about the local symmetry of the Eu^{3+} ion, the emission spectra of the $EuZrF_7$ polycrystal has been measured and compared in Fig. 10 with that of the fluorozirconate GC. The great similarities of both spectra experimentally supports the hypothesis of Adam *et al.*,[5] Lucas *et al.*[6] and Poulain *et al.*[21] that considered this crystalline phase as the "parent structure" for the Eu^{3+} environments in the precursor fluorozirconate glass.

Excitation spectra for both GC and $EuZrF_7$ polycrystal, in the range from 550 to 580 nm and monitoring the $^5D_0 \rightarrow {}^7F_2$ emission at 615 nm also confirm this similarity (see Fig. 12). As it shown in this figure, a small difference (~ 15 cm^{-1}) exists in the energetic position of the $^5D_0$ level, being at about 578.25 nm for the $EuZrF_7$ phase while it is at

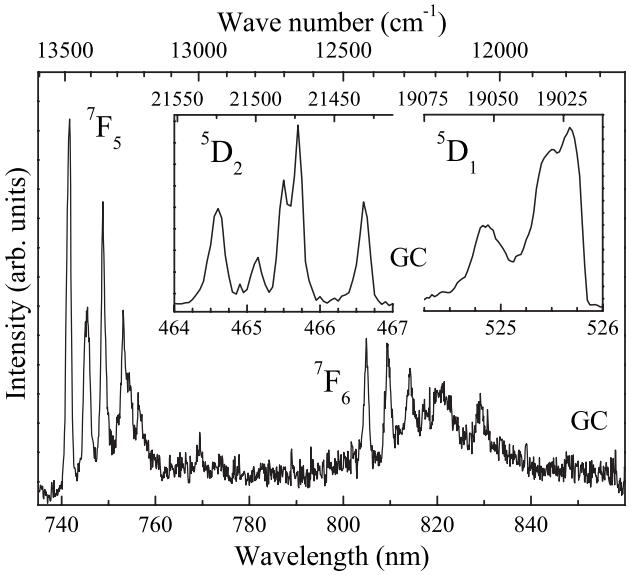

FIG. 11. $^5D_0 \rightarrow {}^7F_J$ ($J=5,6$) emission and $^7F_0 \rightarrow {}^5D_J$ ($J=1,2$) excitation spectra in a fluorozirconate GC doped with 2.5 mol % of Eu^{3+} ions at 13 K. The spectral resolution is 0.05 nm.

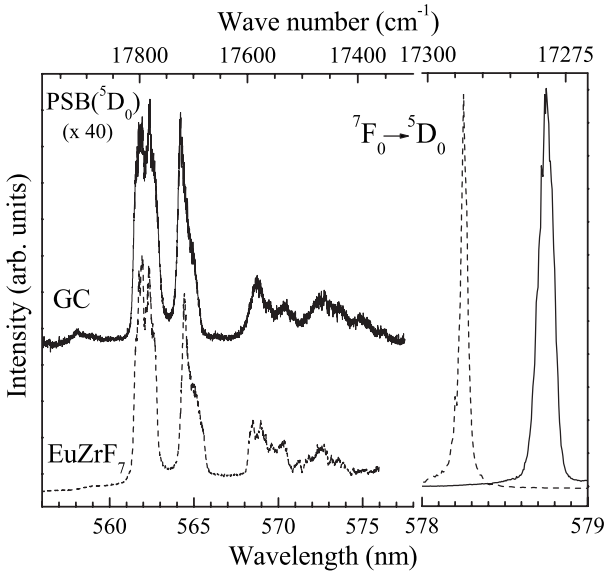

FIG. 12. $^7F_0 \rightarrow {}^5D_0$ excitation spectra in a fluorozirconate GC doped with 2.5 mol % of Eu^{3+} ions and in an $EuZrF_7$ polycrystal at 13 K. The spectral resolution is 0.15 cm^{-1}.

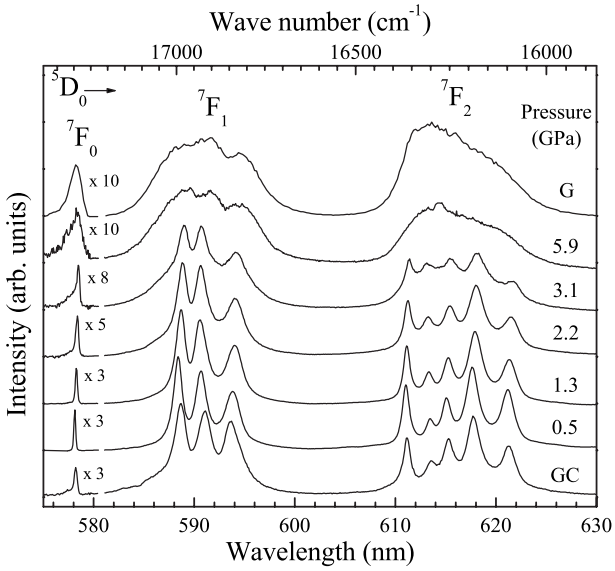

FIG. 13. Evolution with pressure (in GPa) of the $^5D_0 \rightarrow {}^7F_J$ ($J=0-2$) emission spectra in an $EuZrF_7$ crystal at RT. Fluorescence from the Eu^{3+} ions in fluorozirconate glass (G) and GC at RT are included for comparison. Spectra are normalized to the maximum intensity of the $^5D_0 \rightarrow {}^7F_1$ transition and the spectral resolution is 0.2 nm.

about 578.75 nm for the fluorozirconate GC. The PSBs associated to the $^7F_0 \rightarrow {}^5D_0$ transition also show similar line profiles and relative intensities, especially for the high-energy band associated to $Eu^{3+}-F^-$-ligand vibrational modes of maximum energies of about 450 and 520 cm^{-1}. The energy range without bands between 565.5 and 567.5 nm (330–410 cm^{-1} above the PEB) has been associated in other crystalline matrices to the energy separation between the acoustic and optical phonons. Finally, Adam *et al.*[5] measured a lifetime of 4.9 ms for the $^5D_0$ level in the $EuZrF_7$ polycrystal, quite close to 5.2 ms of the GC under study. From these results, it can be experimentally concluded the existence of only one crystalline local environment for the Eu^{3+} ions with low point symmetry in the GC, identified as that of the $EuZrF_7$ crystal.

C. Pressure-induced crystal-to-glass phase transition

The existence of a parent structure for the Eu^{3+} local structures in the fluorozirconate glass opens new possibilities for developing a structural model for the RE^{3+} ions in this glass. The existence of a distribution of Eu^{3+} environments in the fluorozirconate glass can be explained assuming a continuous distortion of the $EuZrF_7$ structure. Distortions generate a large variety of environments for the Eu^{3+} ions with different distances and bond angles with the fluoride ligands, giving rise to different CFs and, as a consequence, to small variations in the energy level scheme and the optical properties of the Eu^{3+} ions.

This hypothesis can be experimentally supported by applying high-pressure techniques. The idea is exploring the reverse change, from crystalline to glassy environment for the Eu^{3+} ions, using a DAC and applying increasing pressure to the $EuZrF_7$ crystals.

The $^5D_0 \rightarrow {}^7F_J$ ($J=0-2$) emission spectra of the Eu^{3+} ions in $EuZrF_7$ polycrystal measured at different pressures at RT are presented in Fig. 13. For 0.5 GPa the emission is similar to that found for the fluorozirconate GC. A slight redshift of the emission is observed when pressure is increased, along with a decrease of the emission and a broadening of the peaks. The latter effect indicates the occurrence of amorphization and begins to be clearly observed in the $^5D_0 \rightarrow {}^7F_0$ transition above 2.2 GPa. With increasing pressure the relative intensity of the sharp peak, originating from Eu^{3+} ions in the $EuZrF_7$ phase, decreases compared to the broad shoulder that appears at the high-energy side of the $^5D_0$ band. This broad band is associated to Eu^{3+} ions with higher transition probabilities and blueshifted $^5D_0 \rightarrow {}^7F_0$ transition energies in stronger CF environments. Both effects can be explained as due to the J-mixing effect[10,20,41,56] since the increase in the wave functions mixing between the $^7F_0$ and the $^7F_2$ multiplets actually shifts the barycenter of the $^7F_0$ levels to lower energies and increase the influence of the larger Ω_2 Judd–Ofelt parameters, as will be shown later.

Amorphization is less clear for the $^5D_0 \rightarrow {}^7F_J$ ($J=1,2$) transitions at relatively low pressures. However, an abrupt change is observed between 3.1 and 5.9 GPa, similar to the case of the $^5D_0 \rightarrow {}^7F_0$ transition. As before, these results indicate an increase in the fluctuation of the local structures due to differences in the $Eu^{3+}-F^-$ bond distances and angles. Finally, the amorphization process finishes above 5.9 GPa and no further change is observed in the line profile of these emissions.

The Eu^{3+} emission spectrum in the fluorozirconate glass is also included in Fig. 13. Compared to the luminescence of the $EuZrF_7$ crystalline phase at 5.9 GPa, large similarities are observed for the $^5D_0 \rightarrow {}^7F_J$ ($J=0,1$) transitions, indicating that the distribution of environments for the Eu^{3+} ions are comparable for both samples. Differences are observed in the intensity and line shape of the hypersensitive $^5D_0 \rightarrow {}^7F_2$ transition that could be related to the different compositions of the precursor glass and the $EuZrF_7$ crystal that slightly alters

the Eu^{3+} local structure. The value of the $^5D_0 \rightarrow {}^7F_2/{}^5D_0 \rightarrow {}^7F_1$ intensity ratio is around 0.9 for the $EuZrF_7$ polycrystal at 5.9 GPa, and it is comparable to the value of around 1.2 found for the fluorozirconate glass.

These results suggest that the changes in the Eu^{3+}–F^- distances and bonds of the $EuZrF_7$ crystal environment could explain the distribution of environments found in the fluorozirconate glass for the Eu^{3+} ions. The distortions suffered by the parent structure are not severe for the ions in weak CF Eu^{3+} environments, whereas the changes must be increasingly larger for medium CF environments. On the other hand, the coordination number is not expected to change drastically from that of the $EuZrF_7$ crystalline phase, since in fluorozirconate glass an average eightfold coordination for the Eu^{3+} ions has been found from EXAFS measurements.[52] Moreover, molecular dynamics studies[19] suggested that the eight-coordinated environments for the Eu^{3+} ions in the fluorozirconate glass could be obtained, between others, from successive distortions or variations of the biccaped trigonal prism geometry found in the $EuZrF_7$ crystal.

V. CRYSTAL-FIELD ANALYSIS

A. Fluorozirconate glass ceramic

The $4f^6$ ground configuration of the Eu^{3+} ion has a total of 3003 Stark levels, but for the fluorozirconate GC with a $EuZrF_7$ phase as local structure of the Eu^{3+} ions, only up to 44 Stark levels have been experimentally measured. This fact is quite common and is usual to apply some kind of truncation of the wave functions. Taking advantage of the almost pure Russell–Saunders character of the wave functions of the ^7F_J multiplets, a standard first approach in the CF analysis of Eu^{3+}-systems is to analyze only the 49 ^7F_J Stark levels and consider the ^7F_J barycenters as adjustable parameters, in order to take into account the full J-mixing effect.

Because some of the ^7F_J $(J=5,6)$ Stark level positions are not obtained from the experiments, this approach was performed in two steps. First, taking the *ab initio* set of CF parameters as starting parameters and fitting all the 25 experimental ^7F_J $(J=1-4)$ Stark levels. Second, once these levels have been fitted and with the calculated CF parameters, the rest of 10 ^7F_J $(J=5$ and $6)$ experimental Stark levels have been included in order to obtain a good fit (rms around 6 cm^{-1}) for the 35 Stark levels observed in the ^7F term. Table I (labeled A and B) reports two different final sets of CF parameters and ^7F_J barycenters obtained after successive calculations. These sets are two examples of fitting that only differ in the values of the nonaxial CF parameters of rank 6 to give the same Stark energy level fitting. However, the second and fourth rank CF parameters (see Table I in bold) only show small changes due to a compensation process in the fitting. The total scalar CF strength parameter, S, and the relative contributions, $\%S^{(k)}$, are also included in this Table. The experimental and calculated energies of the ^7F_J Stark levels are given in Table II (labeled A and B).

A more developed approach is diagonalizing the Eu^{3+} free ion and the CF Hamiltonian within the intermediate scheme. This approach will let include the ^5D_J Stark levels in the fitting process. However, the determination of the free-ion Hamiltonian needs a large number of $^{2S+1}L_J$ multiplets, but optical measurements usually allow the experimental determination of only the lowest multiplets. As a consequence, there must be a restriction in the number of parameters used in the diagonalization of the free-ion Hamiltonian. In this study only those parameters with a major influence in the energetic positions of the ^7F_J and ^5D_J multiplets were used. Thus the Slater (using the hydrogenic approximation) and the spin-orbit parameters are the only ones allowed to vary in the fitting process, and the rest of free-ion parameters were fixed at averaged values commonly used for Eu^{3+}.[10] The Stark energy level diagram of the Eu^{3+} ion in the GC has been simulated, taking as starting CF parameters those previously obtained using only the ^7F_J multiplets. The final set of atomic and CF parameters reported in Table III is considered to give the best fit between the 44 experimental levels and the calculated ones. The results obtained in this fitting are given in Table II (labeled C), along with their irreducible representations obtained from the symmetry of the calculated Stark wave functions. The rms deviation for the final fit is around 18 cm^{-1}, indicating a good agreement between the experimental and calculated Stark levels, as can be seen in Fig. 14. Moreover the ^7F_J energy barycenters obtained from the atomic parameters coincides, in practice, with those obtained from the previous fit using the first approach, indicating that only small inaccuracies are introduced by the approximated (with only two adjustable parameters) free-ion wave functions.

Due to the fact that this is a highly nonlinear calculation, and because the absence of several experimental levels from the ^7F_J $(J=5,6)$ multiplets, not all the CF parameters have been calculated with the same accuracy. Some of them may be varied in a wide range of values without giving rise to significant changes in the energetic positions of the calculated Stark levels. Actually, some parameters only have a major influence in some determined levels, such as the dependency of the $^7F_1$ Stark levels on the B_q^2 parameters.

The degree of sensitivity of every Stark level to the variation of each CF parameters could give an idea of the uncertainty in the calculation of these parameters in the $EuZrF_7$ phase. However, due to the large number of CF parameters for the C_S symmetry, the analysis of this sensitivity is not an easy task, and one may wonder if the dependence of a given Stark level with the B_q^k parameters could be stated. That is why this analysis has been done taking into account all the CF parameters, real and imaginary, of the same rank k. In Table II is indicated the sensitivity of every ^7F_J and ^5D_J Stark level to the second, fourth, and/or sixth ranks CF parameters if their energetic positions change at least 15 cm^{-1} when all the parameters of the same rank vanish.

The results are quite surprising since, apart from the $^7F_1$ Stark levels, the B_q^2 parameters mainly affect to the $^7F_5$ and $^7F_6$ Stark levels, while the sensitivity to the B_q^6 parameters is only manifested by the $^7F_5$ Stark levels and the low-energy $^7F_4$ Stark level. Moreover, the dependency of almost all the Stark levels with the B_q^4 parameters, and specially their influence in the overall splitting of the $^7F_1$ multiplets, indicates

TABLE II. Experimental and calculated ^7F_J (J=0–6) and ^5D_J (J=0–3) Stark levels (in cm^{-1}) of the Eu^{3+} ion in a fluorozirconate GC. Sets A and B of Stark energy levels are obtained diagonalizing only the ^7F_J multiplets while set C includes also the ^5D_J multiplets (see text).

$^{2S+1}L_J$ (degeneracy)	Experimental Stark levels	Calculated levels			Irreducible representation C_S symmetry
		A[a]	B[b]	C[c]	
$^7F_0$ (1)	0	0	0	10	A'
$^7F_1$ (3)	312[d,e]	315	308	323	A''
	371	365	370	375	A'
	448[d,e]	452	455	464	A''
$^7F_2$ (5)	927[d]	929	929	922	A''
	987[e]	981	994	982	A'
	1037[e]	1037	1030	1039	A''
	1104	1106	1100	1102	A'
	1195[e]	1198	1197	1203	A'
$^7F_3$ (7)	1874[e]	1878	1878	1872	A''
	1887	1889	1887	1880	A'
	1900[e]	1898	1899	1885	A''
	1914	1916	1918	1913	A''
	1951	1948	1948	1940	A'
	1978[e]	1979	1978	1970	A'
	2002[e]	1997	2000	1995	A''
$^7F_4$ (9)	2737[e,f]	2736	2741	2737	A'
	2789[e]	2790	2787	2789	A'
	2810[e]	2812	2806	2797	A''
	2833[e]	2839	2833	2837	A'
	2912	2903	2910	2898	A''
	2954[e]	2957	2955	2958	A'
	2997[e]	2993	2991	2995	A''
	3021[e]	3023	3023	3020	A'
	3041[e]	3040	3043	3035	A''
$^7F_5$ (11)	3796[e,f]	3795	3791	3802	A''
	...[e]	3815	3808	3815	A'
	...[e,f]	3834	3853	3851	A''
	3864[e,f]	3855	3862	3859	A''
	...[e]	3907	3879	3894	A''
	3925[d]	3926	3927	3928	A'
	...	3946	3952	3944	A'
	4001	4009	4007	4004	A''
	...[e,f]	4025	4035	4041	A'
	4061[d,e]	4054	4060	4063	A''
	...[d–f]	4063	4071	4071	A'
$^7F_6$ (13)	4856[d,e]	4863	4861	4867	A''
	...[d,e]	4867	4861	4868	A'
	4926[e]	4919	4920	4923	A'
	...[e]	4923	4926	4925	A''
	...[e]	4982	4991	4996	A''
	4998	4995	4996	5005	A'
	...[e]	5036	5047	5054	A''
	...[d,e]	5068	5095	5089	A'
	5098[d,e]	5102	5103	5110	A'
	...[e]	5121	5113	5127	A''
	...[e]	5132	5118	5137	A'
	5220[d,e]	5215	5215	5223	A'
	...[d]	5215	5215	5223	A''
$^5D_0$ (1)	17 288	...	...	17 304	A'

TABLE II. (*Continued.*)

$^{2S+1}L_J$ (degeneracy)	Experimental Stark levels	Calculated levels A[a]	B[b]	C[c]	Irreducible representation C_S symmetry
$^5D_1$ (3)	19 024	···	···	19 005	A''
	19 029	···	···	19 018	A'
	19 053	···	···	19 046	A''
$^5D_2$ (5)	21 432	···	···	21 454	A'
	21 473	···	···	21 479	A'
	21 482	···	···	21 482	A''
	21 498	···	···	21 495	A'
	21 524	···	···	21 515	A''
$^5D_3$ (7)	···	···	···	24 362	A'
	···	···	···	24 373	A''
	···	···	···	24 383	A'
	···	···	···	24 387	A''
	···	···	···	24 393	A''
	···	···	···	24 406	A''
	···	···	···	24 407	A'

[a]Values from the CF parameters (A) in Table II.
[b]Values from the CF parameters (B) in Table II.
[c]Values from the atomic and CF parameters in TableIII.
[d]Indicates a large dependency of the Stark level with the B_q^2 CF parameters.
[e]Indicates a large dependency of the Stark level with the B_q^4 parameters.
[f]Indicates a large dependency of the Stark level with the B_q^6 parameters.

the importance of the CF strength in the middle range of Eu^{3+}–F^- distances, indicating a high degree of covalency found for, *a priori*, an ionic and weak CF environment like that of the $EuZrF_7$ crystalline phase. Changes in the ^5D_J Stark levels are less important due to the weaker influence of the CF interaction. As a conclusion, the second and fourth rank CF parameters have been calculated with higher accuracy than the sixth rank ones, whose influence in the splitting in the $EuZrF_7$ crystalline phase is much weaker.

The final question the authors ask themselves is about the physical meaningful of the "final set of parameters" given in Table III. It should be remarked that all the B_q^6 nonaxial ($q \neq 0$) parameters are very poorly determined due to small number of Stark levels in the $^7F_5$ and $^7F_6$ multiplets. Only a few CF parameters (mainly those marked as bold in Table I) could be taken as "properly determined." Even though these inaccuracies seem to compromise the obtained results, the authors still trust on the general validity of this

TABLE III. Atomic and CF parameters in an Eu^{3+}-doped fluorozirconate GC (in cm^{-1}). Errors are indicated in parenthesis (in cm^{-1}). The hydrogenic approximation (see footnote) has been taken for the Slater parameters F^k and those values in brackets have been taken from Görller-Walrand and Binnemans (Ref. 10) and have been fixed during the fitting process.

Atomic parameters		CF parameters	
E_{av}	65 435	B_0^2	−85(17)
F^2 [a]	87 027 (13)	B_2^2	−286(15)
ζ_{4f}	1333 (3)	B_0^4	−983(24)
α	[19.8]	B_2^4	−223(29)
β	[–617]	$B_2'^4$	−594(24)
γ	[1460]	B_4^4	416(26)
$T2$	[370]	$B_4'^4$	55(34)
$T3$	[40]	B_0^6	−157(30)
$T4$	[40]	B_2^6	−221(33)
$T6$	[–330]	$B_2'^6$	−228(33)
$T7$	[380]	B_4^6	−52(29)
$T8$	[370]	$B_4'^6$	115(28)
$M0$ [a]	[2.38]	B_6^6	77(25)
$P2$ [a]	[245]	$B_6'^6$	−66(33)

[a]$F^4/F^2=0.668$ and $F^6/F^2=0.4943$, $M^2/M^0=0.56$ and $M^4/M^0=0.38$, and $P^4/P^2=0.75$ and $P^6/P^2=0.5$.

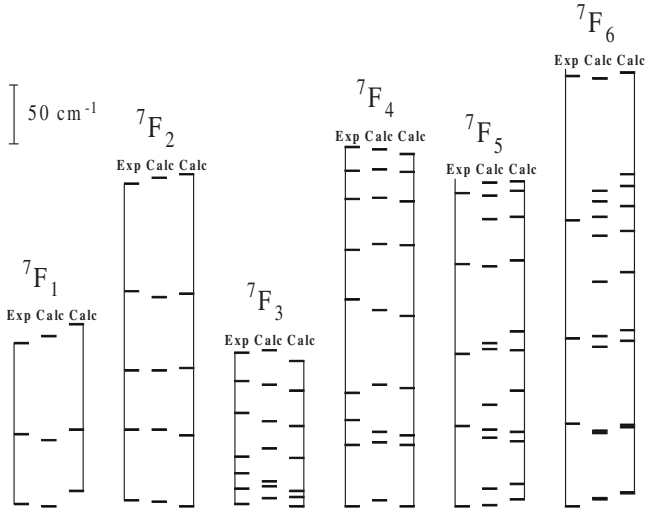

FIG. 14. Experimental (left) and calculated (central and right) ^7F_J ($J=1-6$) Stark levels of the Eu^{3+} ion in the $EuZrF_7$ crystal. The central fit corresponds to the CF parameters in Table I(a) and the right hand fit to the CF parameters in Table III.

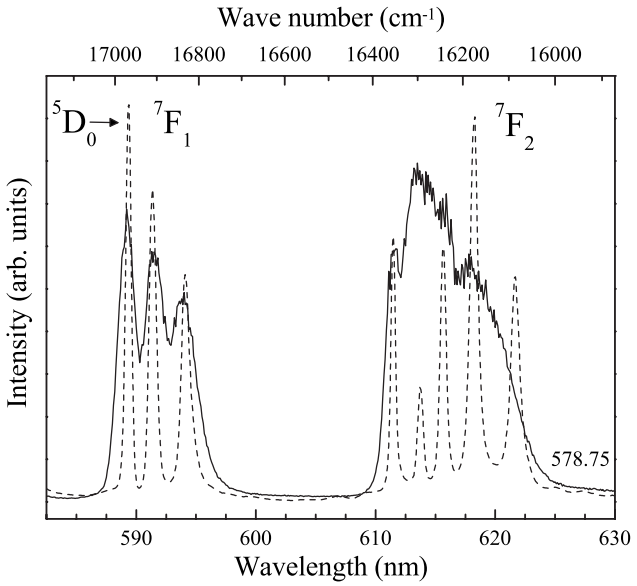

FIG. 15. $^5D_0 \rightarrow {}^7F_J$ $(J=1,2)$ emission spectra in a fluorozirconate glass (solid; exciting at 578.75 nm) and GC (dash) doped with 2.5 mol % of Eu^{3+} ions at 13 K.

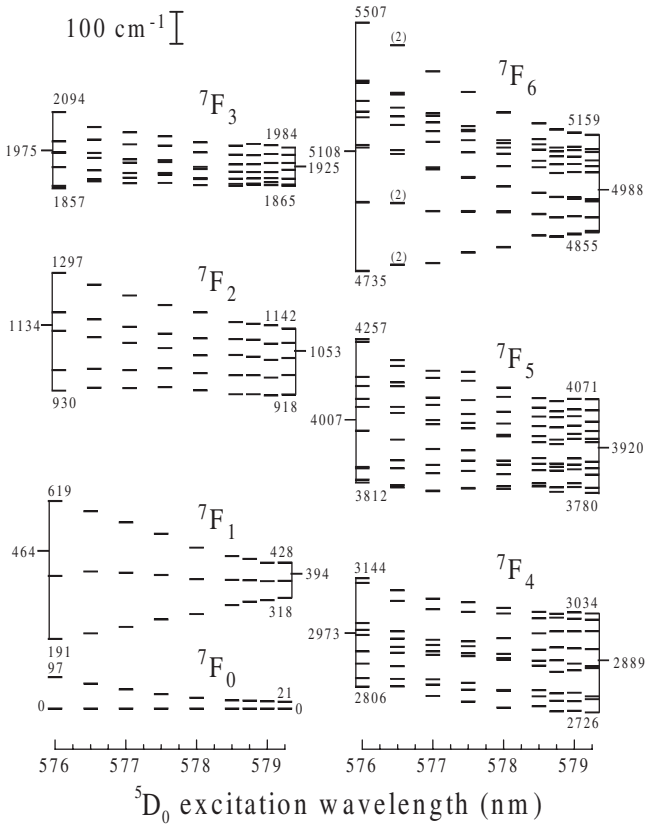

FIG. 16. Simulation of the ^7F_J $(J=0-6)$ Stark energy level diagram in the Eu^{3+}-doped fluorozirconate glass as a function of the $^5D_0$ excitation wavelength. In the $^7F_6$ multiplet, (2) indicates two close Stark levels. Numbers indicate the barycenters and maximum splitting of the ^7F_J multiplets in the strongest and the weakest Eu^{3+} local environments of the fluorozirconate glass.

approach since the obtained scalar CF strength parameters S and the $\%S^{(k)}$ $(k=2,4,6)$ relative contribution have similar values for both A and B approximations, as shown in Table I. This means that the "nonproperly determined" CF parameters changes in such a compensated way that the rotational invariant CF strength parameter, remains unchanged. Thus the strategy to follow should focus on the behavior of the properly determined CF parameters and on the S parameter and its relative variations $\%S^{(k)}$.

B. Fluorozirconate glass

Once the GC is fitted, the following step in the simulation procedure is the attempt to calculate the CF interaction in the glass, obtaining their CF parameters for all the Eu^{3+} local environments from those already obtained for the GC. Thus the first point that should be clearly stated is in which particular local structure in the glass the Eu^{3+} ions feel similar CF strength as in the $EuZrF_7$ local crystalline structure.

As already mentioned, there is a range of excitation, in the low-energy side of the $^7F_0 \rightarrow {}^5D_0$ band, for which only predominantly weak CF environments are excited and there are only small changes from one environment to the other. Only for laser excitations below 577.5 nm the CF becomes increasingly stronger, reaching medium CF strengths. The same behavior can be observed in the site-selective lifetime and in the relative intensities of the electric-dipole transitions. Supported by these facts, the emission spectra obtained for the $^5D_0 \rightarrow {}^7F_J$ $(J=1,2)$ transitions in the $EuZrF_7$ crystalline phase and in those environments of the glass excited at around 578.75 nm (weak CF) are compared in Fig. 15. The similar splitting and CF strength obtained for the $^7F_1$ and $^7F_2$ Stark levels let us identify the last one as the Eu^{3+} environment whose local structure in the glass is much closer to the crystalline phase. Thus the weak CF environments must be similar to those found for the $EuZrF_7$ crystal (see Fig. 1), in which the Eu^{3+} ions are surrounded by 8 fluorine ions.

The method of calculation is simple. As the starting point of the CF analysis of the fluorozirconate glass, the set of CF parameters of the $EuZrF_7$ phase is used as the *ab initio* CF parameters for the simulation of the Stark levels obtained exciting the $^7F_0 \rightarrow {}^5D_0$ band at 578.5 nm. The process continues in such a way that the final set of CF parameters obtained for a certain Eu^{3+} environment is taken as the initial one for the calculation of the CF parameters for the next closer Eu^{3+} environment, following an increasing magnitude of the CF strength.

However, the main problem is again the short number of Stark levels experimentally obtained. The $^7F_1$ Stark levels are relatively easy to obtain for all the excitation wavelengths of interest and the five $^7F_2$ Stark levels have been obtained from the Gaussian deconvolution of the fluorescence spectra, as it is shown in Fig. 7 for different $^5D_0$ excitation wavelengths. For the rest of ^7F_J multiplets it is often possible to obtain with relative accuracy only the energy position of the lowest Stark level and, occasionally, a few higher energy level positions. Due to these features, the RECFCALC program enforces the fit of those experimentally well resolved Stark levels (mainly from $^7F_1$ and $^7F_2$ manifolds) through a weighted factor in the fitting process.

The calculated ^7F_J Stark level positions are shown in Fig. 16. A fairly good agreement from calculated to the experimental data is obtained, although the approximation fol-

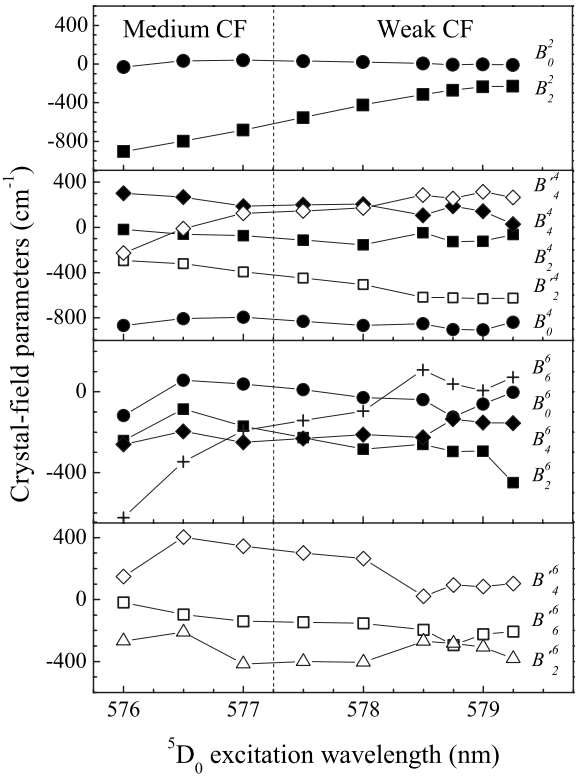

FIG. 17. CF parameters, B_q^k and $B_q'^k$, as a function of the excitation wavelength in an Eu^{3+}-doped fluorozirconate glass.

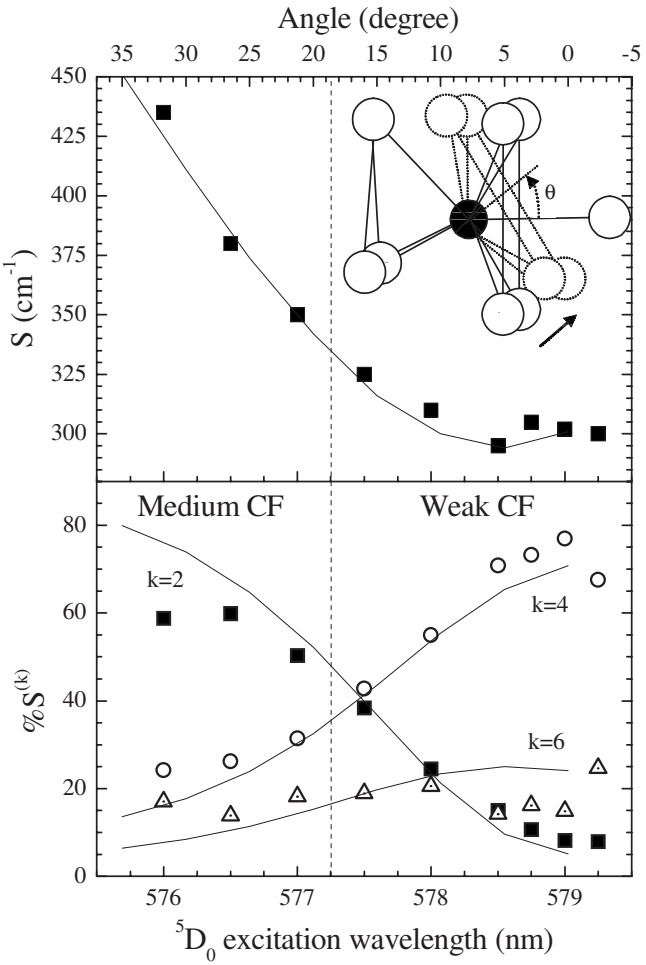

FIG. 18. Fitted scalar CF strength parameter (upper), and their second, fourth, and sixth rank contributions, as a function of the $^5D_0$ excitation wavelength in an Eu^{3+}-doped fluorozirconate glass. Solid lines are the calculated evolution of their values as a function of the angle of tilting of the square plane in the idealized structure. The inset shows a *z*-view of the idealized structure showing the direction of rotation used in the simulation.

lowed in the fitting process may seem to rest accuracy to these results. In particular the fitting accurately reproduces the ^7F_J splitting observed from the site-selective emission spectra. As an example, using the calculated Stark energy level diagram it has been included in Fig. 5 the energies of the emissions from the $^5D_0$ level to the different ^7F_J ($J=3-5$) Stark levels, together with the FLN emission spectra to the ^7F_J ($J=3-5$) multiplets, showing a quite good agreement between the experimental and the calculated energy levels. It is also worth noting that the calculated CF parameters explain the almost independent splitting of the $^7F_4$ multiplet with the laser excitation wavelength.

The evolutions of the CF parameters as well as the scalar CF strength parameters are depicted in Figs. 17 and 18, respectively. From these figures, the evolution of the distortion from weak to medium CF environments is described by a monotonic, nonlinear increase in the scalar CF strength from around 300 to 435 cm^{-1}. It is worth noting that this increase is mainly ruled by the orthorhombic B_2^2 parameter that also suffers a monotonic increase (in absolute value), whereas axial parameters, B_0^k ($k=2,4,6$), do not suffer significant variations. The observed changes in other parameters appear more arbitrary and are difficult to understand, mainly in the poorly determined CF parameters.

In order to clarify in some way the obtained results, attention is paid to the relative contribution of the rank k rotationally invariant CF strength $\%S^{(k)}$ ($k=2,4,6$) parameters, whose relative evolutions are displayed in Fig. 18. As can be seen, in weak CF environments the $\%S^{(2)}$ contributes in only 10% to the total CF value and this value increases to 60% in medium CF environments, the $\%S^{(4)}$ percentage is reduced from 80% to 20%, and finally the sixth rank CF parameters gives a low, and almost constant, contribution to the total CF strength (10%–20% of the total CF strength parameter). Thus we can clearly state that second and fourth rank relative variation are the main responsible for the observed CF changes, while only a very small variation in the $\%S^{(6)}$ contribution is observed. Since 6-rank parameters are related with very short distances, this result would support the idea of a unique kind of site for the Eu^{3+} ions in fluorozirconate glasses.

The above results indicate that, as it was observed for the $EuZrF_7$ crystalline phase, there is a high contribution of the four-rank CF parameters through the whole distribution of weak CF environments in the fluorozirconate glass. Since the CF parameters show an $R^{-(k+1)}$ dependence with the distance [see Eq. (10)] from the central Eu^{3+} ion, the large $\%S^{(4)}$ values indicate that the main contribution to the overall electrostatic energy of the Eu^{3+} bonding environment, i.e., the CF interaction, comes from middle range distances between the Eu^{3+} ions and its ligands. This would confirm a high degree of covalency of the $Eu^{3+}-F^-$ bonds in the weak CF environments. Moreover, the main influence of the CF con-

tinuously change to farer distances from the Eu^{3+} ion when the medium CF environments are reached, showing a higher contribution of the 2-rank and indicating a more ionic character of the $Eu^{3+}-F^{-}$ bonds. These results are quite surprising since it follows a similar trend found for the Eu^{3+} ion by Lochhead and Bray[57] and Monteil *et al.*[58] in silicate oxide glasses using high-pressure FLN and molecular dynamics techniques, respectively, although a more ionic character would be expected in a fluoride glass.

On the other hand, if the even CF strength increases with the excitation energy, one should expect the same trend for the odd CF parameters. Thus the variety of local structures in the fluorozirconate glass should show different transitions probabilities for different Eu^{3+} environments. Thus the variations of the Ω_2 intensity parameter is only increasingly important for those Eu^{3+} ions in medium CF environments and may explain the asymmetry in the line profile in the high-energy side of the $^7F_0 \rightarrow {}^5D_0$ PEB as due to larger absorption transition probabilities. Moreover, since the oscillator and line strengths of this transition only depend on the Ω_2 Judd–Ofelt parameter, through *J*-mixing,[56,59] and on the number of ions in the ground state at low temperature, an estimation of the fraction of Eu^{3+} ions in weak and medium CF environments has been calculated. It can be concluded that around 75% of Eu^{3+} ions occupy weak CF environments whereas the rest, around 25%, are incorporated in medium CF environments.

VI. GEOMETRICAL LOCAL STRUCTURE MODEL

It is possible to analyze the Eu^{3+} local environments in the fluorozirconate glass following the trend of the CF strength from weak to medium values by a continuous modification or distortion of the EuF_8 polyhedra of the idealized $EuZrF_7$ structure. The nature and magnitude of this distortion can be extracted from the calculated CF parameters, although some empirical assumptions must be followed in order to constrain the numerous possible structures that can be found. In the following it is assumed that Eu^{3+} local structures resulting from the successive distortions with respect to the idealized structure may have a point symmetry at least as low as the C_S symmetry of the $EuZrF_7$ phase and their coordination number would not differ significantly from the eightfold coordinated Eu^{3+} ions found in the crystalline phase. Moreover, and taking into account the low symmetry of the Eu^{3+} local structures in the glass, a further condition imposed to the geometrical model is that simple distortions of the crystalline structure should explain the obtained changes of the CF parameters.

As pointed out by Lochhead and Bray,[57] the developing of a structural model based on FLN measurements has been questioned. Different simulations in fluoride[19] and oxide[60] glasses suggest that the accidental degeneracy may be more significant than it was initially considered, with multiple Eu^{3+} local geometries yielding the same $^7F_0 \rightarrow {}^5D_0$ energy. Thus the intention of this work is giving a qualitative description of the average distribution of Eu^{3+} environments in the fluorozirconate glass that could be consistent with the experimental data.

On this frame, the SOM model has been used to calculate the CF parameters for the continuous geometrical rearrangements of the EuF_8 polyhedra in the range form weak to medium CF strength values (300–435 cm^{-1}). Different kinds of deformations have been investigated that permit to follows the obtained behavior of the total CF strength parameter including compression and deformations of the local structure. As a first step in this study, a simulation of a hydrostatic compression without deformation was calculated. This simulation easily reproduces the trend of the *S* value increasing from 300 to 435 cm^{-1} with only a very small reduction ($\approx$4%) of the host volume but, obviously, the relative values of the $\%S^{(k)}$ parameters remains unchanged because they are related with the relative amount of the CF strength associated to different $Eu^{3+}-F^{-}$ bond distances. Thus it is necessary to rearrange the local structure to reproduce the observed variation in the relative $\%S^{(k)}$ parameters.

Extensive computational work has been achieved to check several variations of the idealized structure of the Eu^{3+} first coordination sphere of ions that may reproduce the observed trend of the *S* and $\%S^{(k)}$ CF parameters. Excellent results are obtained with a systematic deformation of the idealized structure in which the fluorine ions forming the square in the idealized structure suffer a *z*-axis rotation around the central Eu^{3+} ion, without changing the $Eu^{3+}-F^{-}$ bond distances. The results of this simulation are reported as solid lines in Fig. 18. The inset in this figure show a *z*-view of the idealized structure in which the rotation is indicated. From the CF point of view it can be stated that the relative location of the four fluorine ions forming the square appears as the main responsible of the relative values of the nonaxial CF parameters. In particular, by tilting this square as indicated in Fig. 18, a rapid increase in the absolute value in the orthorhombic, B_2^2, parameter without any changes in the axial parameters, B_0^k ($k=2,4,6$) is obtained, in the same way as it observed in the reported fitting of the experimental data. As can be seen in Fig. 18, the calculations reported are in excellent agreement with the observed trend of the total CF strength *S* and the $\%S^{(k)}$ parameters from weak to medium CF strength values.

Although it has been pointed out the high degree of uncertainty in the values of the CF parameters, the goal of this description is to properly reproduce the strong crossing changes observed in the relative contribution of the two- and four-rank CF parameters and the increasing of the total CF strength parameter in such an easy way.

Finally, from the structural point of view it could be assumed that such a tilting imply a slight reduction of the EuF_8 volume in the overall structure. If we assume that the sharing edges ZrF_6 complex (see Fig. 1(b)) also turns without additional distortion absorbing the deformation, we may conclude that a slight increase of density is taking place (estimated at the most as 2% of volume cell) from weak to medium CF strength values. Any other structural conclusion, including changes in the "effective" coordination number appears as quite speculative and can be disregarded.

VII. SUMMARY AND CONCLUSIONS

Glasses are characterized by a short-range order and a long-range disorder. In heavy metal fluoride glasses, the ZrF_4 acts as a network forming whereas the BaF_2, due to its large size, as a network modifier, allowing the Zr^{4+} to have a large variety of polyhedra with extremely variable Zr–F–Zr angles due to the presence of bridging and nonbridging fluorine ions. On the other hand, the Al^{3+} and the Y^{3+} ions are good stabilizers of the fluorozirconate glass, decreasing the crystallization rate and increasing the compactness occupying octahedral sites for Al^{3+} and close to the ZrFn polyhedra, but larger, for the Y^{3+}. Thus the vitreous network is constructed from the association of the ZrF_n ($n=6$, 7, and 8) polyhedra sharing corners or edges.

The short distribution of local environments for the optically active ions support the conclusion that they may act as former or intermediate ions in the fluorozirconate glass, being able to be in and out of the network positions. The Eu^{3+} ions demand and obtain from the network a particular sphere of coordination to reach the charge neutrality, predominantly bonding with the bridging and, to a lesser extent, with the nonbridging fluorine ions of the ZrF_n units. These fluorine ions will form the first coordination sphere, adding a local charge that will balance the +3 charge of the Eu^{3+} ions, while the rest of former and modifier ions will incorporate in the successive spheres, balancing the excess of charge of the fluorine ions. The Eu^{3+} ion achieve the charge neutrality with an average eight coordination number, typical for lanthanides in heavy metal fluoride glasses due to the ionic radius of the fluoride and the Eu^{3+} ions.

These features generate a variety of environments for the Eu^{3+} ions with slightly different distances and bond angles with the fluorine ligands, giving rise to different CFs ranging from weak to medium strength and, as a consequence, to small variations in the energy level scheme and the optical properties of the Eu^{3+} ions. The main difference with the oxide glasses is that the local structure and the CF strengths distributions are significantly lower in fluoride glasses. Nearly 75% of the Eu^{3+} ions in the glass occupy weak CF environments with shorter Stark splitting, larger decay times and quite similar geometrical local structure and absorption and emission probabilities. The rest of Eu^{3+} ions, around 25%, are occupying medium CF environments with higher local asymmetry, greater Stark splitting and shorter decay times. No strong CF environments similar to those of oxide glasses have been found.

However, the site-selective experimental results indicate the existence of a unique kind of site in this glass, being suggested by different authors the existence of a parent structure for the fluorozirconate glass, which could be the $EuZrF_7$ crystalline phase.

Following a crystal-chemistry approach, the temperature-induced crystallization of the glass and the pressure-induced amorphization of the crystalline $EuZrF_7$ have played a relevant, and decisive, role giving the experimental evidence that a distortion of the geometrical parent structure can explain the distribution of local environments for the Eu^{3+} ions in the fluorozirconate glass. In the first phase transition process, a thermal treatment of the fluorozirconate glass near the temperature of crystallization induces the precipitation of microcrystals in the glassy phase, giving rise to the so-called GC. By this means almost all the Eu^{3+} ions enter into a crystalline phase identified as the $EuZrF_7$ one. In the second induced phase transition, experimental evidence of the reverse change, from a crystalline to a glassy distribution of environments for the Eu^{3+} ions, has been also obtained combining optical spectroscopic and high-pressure DAC techniques to analyze the pressure-induced amorphization of the $EuZrF_7$ crystal.

The FLN technique gives experimental valuable data to analyze the CF parameters, energy levels, lifetimes and energy transfer processes between Eu^{3+} ions in different environments in the glass. Using CF theory it has been possible to simulate the ^7F_J ($J=0-6$) Stark energy level diagram of the Eu^{3+} ions in all the local environments found in the fluorozirconate glass.

As pointed out by Brecher and Riseberg, the excitation dependent pattern of the Stark splittings and the structural model proposed as a physical rationalization reflect only an average behavior for the distribution of local environment for the Eu^{3+} ions in the glass. However, a simple geometrical model that could reproduce the CF parameters, and hence the energy level diagram and transition probabilities, can be generated. This geometrical model, which involves only the use of the EuF_8 polyhedra in a very simple idealized local structure, predicts, with reasonable accuracy, the CF interaction over the Eu^{3+} ions in the fluorozirconate glass, allowing studying the correlation between their optical properties and the local environments where they reside. The main distortion responsible of the variations of CF felt by the Eu^{3+} can be correlated with changes in the relative position of four fluorine ions, forming a square that tilts around the central Eu^{3+} ion without any change in their distances. The distortion seems not to be so severe for the Eu^{3+} ions in weak CF environments, and is increasingly higher for those Eu^{3+} ions in medium CF local environments in the fluorozirconate glass.

ACKNOWLEDGMENTS

Dr. Víctor Lavín is grateful to Dr. Muñoz-Santiuste and the rest of members of the Departamento de Física Aplicada (Universidad Carlos III de Madrid) for their hospitality during his stay. This work was supported by the Ministerio Ciencia e Innovación (MAT2007-65990-C03-02, MALTA-Consolider Ingenio 2010 CSD2007-00045 and PCI2006-A7-0638) and EU-Feder funds.

[1] J.-L. Adam, J. Non-Cryst. Solids **287**, 401 (2001); Chem. Rev. (Washington, D.C.) **102**, 2461 (2002).
[2] J. Lucas, J. Fluorine Chem. **72**, 177 (1995).
[3] J. P. Laval, J. Non-Cryst. Solids **161**, 123 (1993) (and references therein).
[4] M. D. Shinn, W. A. Sibley, M. G. Drexhage, and R. N. Brown, Phys. Rev. B **27**, 6635 (1983).
[5] J.-L. Adam, V. Ponçon, J. Lucas, and G. Boulon, J. Non-Cryst. Solids **91**, 191 (1987).
[6] J. Lucas, M. Chanthanasinh, M. Poulain, and M. Poulain, J. Non-Cryst. Solids **27**, 273 (1978).
[7] A. Lecoq and M. Poulain, J. Non-Cryst. Solids **41**, 209 (1980).
[8] W. Wang, Y. Chen, and T. Hu, J. Phys.: Condens. Matter **6**, 2159 (1994).

[9] H. Ebendorff-Heidepriem, I. Szabó, and Z. E. Rasztovits, Opt. Mater. (Amsterdam, Neth.) **14**, 127 (2000).
[10] C. Görller-Walrand and K. Binnemans, in *Handbook of the Physics and Chemistry of Rare Earths*, Vol. 23, edited by K. A. Gschneidner, Jr. and L. Eyring (Elsevier Science B. V., Amsterdam, The Netherlands, 1996), Ch. 155, p. 121.
[11] G. S. Ofelt, J. Chem. Phys. **38**, 2171 (1963).
[12] W. M. Yen and P. M. Selzer, *Laser Spectroscopy of Solids* (Springer-Verlag, Berlín, 1986).
[13] C. Brecher and L. A. Riseberg, Phys. Rev. B **13**, 81 (1976); **21**, 2607 (1980).
[14] G. F. Imbusch, Phys. Scr. **T19**, 354 (1987).
[15] V. Lavín, V. D. Rodríguez, I. R. Martín, and U. R. Rodríguez-Mendoza, J. Lumin. **72–74**, 437 (1997).
[16] R. Balda, J. Fernández, H. Eilers, and W. M. Yen, J. Lumin. **59**, 81 (1994).
[17] K. Soga, M. Uo, H. Inoue, A. Makishima, and S. Inoue, J. Am. Ceram. Soc. **78**, 129 (1995).
[18] V. D. Rodríguez, V. Lavín, U. R. Rodríguez-Mendoza, and I. R. Martín, Opt. Mater. (Amsterdam, Neth.) **13**, 1 (1999).
[19] M. T. Harrison and R. G. Denning, J. Lumin. **69**, 265 (1996) (and references therein).
[20] V. Lavín, P. Babu, C. K. Jayasankar, I. R. Martín, and V. D. Rodríguez, J. Chem. Phys. **115**, 10935 (2001).
[21] M. Poulain, M. Poulain, J. Lucas, and P. Brun, Mater. Res. Bull. **10**, 243 (1975).
[22] M. Poulain, J. Lucas, P. Brun and M. Drifford, Colloques Int. C.N.R.S. **255**, 257 (1977).
[23] M. Poulain, M. Poulain, and J. Lucas, Mater. Res. Bull. **7**, 319 (1972); J. Solid State Chem. **8**, 132 (1973).
[24] Th. Tröster, personal communication (February 2006).
[25] B. G. Wybourne, *Spectroscopic Properties of Rare Earths* (Wiley-Interscience, New York, 1965).
[26] S. Hüfner, *Optical Spectra of Transparent Rare Earth Compounds* (Academic, New York, 1978).
[27] C. A. Morrison and R. P. Leavitt, in *Handbook of the Physics and Chemistry of Rare Earths*, Vol. 5, edited by K. A. Gschneidner, Jr. and L. Eyring (Elsevier Science B. V., Amsterdam, The Netherlands, 1982), Ch. 46, p. 461.
[28] B. R. Judd, Phys. Rev. **127**, 750 (1962); G. S. Ofelt, J. Chem. Phys. **37**, 511 (1962).
[29] R. D. Peacock, Struct. Bonding (Berlin) **22**, 83 (1975).
[30] C. Görller-Walrand and K. Binnemans, in *Handbook of the Physics and Chemistry of Rare Earths*, Vol. 25, edited by K. A. Gschneidner, Jr. and L. Eyring (Elsevier Science B. V., Amsterdam, The Netherlands, 1998), Ch. 167, p. 101.
[31] C. Rudowicz, J. Chem. Phys. **84**, 5045 (1986).
[32] C. Rudowicz and R. Bramsley, J. Chem. Phys. **83**, 5192 (1985).
[33] F. Auzel, Mater. Res. Bull. **14**, 223 (1979).
[34] F. Auzel and O. L. Malta, J. Phys. (Paris) **44**, 201 (1983).
[35] R. P. Leavitt, J. Chem. Phys. **77**, 1661 (1982).
[36] O. L. Malta, Chem. Phys. Lett. **87**, 27 (1982); **88**, 353 (1982).
[37] A. J. Freeman and R. E. Watson, Phys. Rev. **127**, 2058 (1962).
[38] J. E. Muñoz-Santiuste, Rare Earth Crystal-Field CALCulation (RECFCALC) free-software program.
[39] W. T. Carnall, P. R. Fields, and K. Rajnak, J. Chem. Phys. **49**, 4450 (1968).
[40] M. Dejneka, E. Snitzer, and R. E. Riman, J. Lumin. **65**, 227 (1995).
[41] V. Lavín, U. R. Rodríguez-Mendoza, I. R. Martín, and V. D. Rodríguez, J. Non-Cryst. Solids **319**, 200 (2003).
[42] G. Nishimura and T. Kushida, J. Phys. Soc. Jpn. **60**, 683 (1991); J. Phys. Soc. Jpn. **60**, 695 (1991).
[43] M. Tanaka, G. Nishimura, and T. Kushida, Phys. Rev. B **49**, 16917 (1994).
[44] H. Kuroda, S. Shionoya, and T. Kushida, J. Phys. Soc. Jpn. **33**, 126 (1972).
[45] S. Tanabe, S. Todoroki, K. Hirao, and N. Soga, J. Non-Cryst. Solids **122**, 59 (1990).
[46] K. Fujita, K. Tanaka, K. Hirao, and N. Soga, J. Appl. Phys. **81**, 924 (1997).
[47] B. R. Judd, Phys. Scr. **21**, 543 (1980).
[48] S. Todoroki, K. Hirao, and N. Soga, J. Non-Cryst. Solids **143**, 46 (1992).
[49] R. M. Almeida, in *Handbook of the Physics and Chemistry of Rare Earths*, Vol. 15, edited by K. A. Gschneidner, Jr. and L. Eyring (Elsevier Science B. V., Amsterdam, The Netherlands, 1991), Ch. 15, p. 287.
[50] R. M. Almeida and J. D. Mackenzie, J. Chem. Phys. **74**, 5954 (1981).
[51] J. Wang, W. S. Brocklesby, J. R. Lincoln, J. E. Townsend, and D. N. Payne, J. Non-Cryst. Solids **163**, 261 (1993).
[52] Y. Kawamoto, M. Takahashi, K. Ogura, K. Kadono, H. Kageyama, and N. Kamijo, National Laboratory for High Energy Physics KEK (Tsukuba, Japan), Photon activity Report No. 10, proposal No. 92-019.
[53] V. Lavín, I. R. Martin, U. R. Rodríguez-Mendoza, and V. D. Rodríguez, J. Phys.: Condens. Matter **11**, 8739 (1999).
[54] E. W. L. J. Oomen and A. M. A. Van Dongen, J. Non-Cryst. Solids **111**, 205 (1989).
[55] R. Reisfeld, Struct. Bonding (Berlin) **13**, 53 (1973).
[56] G. Nishimura and T. Kushida, Phys. Rev. B **37**, 9075 (1988).
[57] M. J. Lochhead and K. L. Bray, Phys. Rev. B **52**, 15763 (1995).
[58] A. Monteil, C. Bernard, S. Chaussedent, M. Ferrari, N. Balu, and J. Obriot, J. Lumin. **87–89**, 691 (2000).
[59] R. Reisfeld, E. Greenberg, R. N. Brown, M. G. Drexhage, and C. K. Jørgensen, Chem. Phys. Lett. **95**, 91 (1983).
[60] G. Cormier, J. A. Capobianco, C. A. Morrison, and A. Monteil, Phys. Rev. B **48**, 16290 (1993).